3. Results

3.1. FLV + TBI treatment leads to an overexpression of downstream molecules of p in the bone marrow of C3H mice

To address the molecular basis for the *p53*-dependent apoptosis in FLV + TBI-treated C3H mice, downstream molecules of *p53* signaling were analyzed in bone marrow cells using the RT-PCR technique. As expected from the previous observation that p53 was stabilized and accumulated in response to genotoxic stress [1–3], mRNA levels for *p21* and *bax*, both of which were *p53*-target genes, exhibited overexpression after treatment with TBI alone (Fig. 1). However, bone marrow cells from FLV + TBI-treated C3H mice exhibited a much greater expression of *p21* as well as *bax*, in spite that the expression of *β-actin* mRNA was a little weaker in FLV + TBI-treated sample. These results suggested that genes encoding downstream molecules of *p53* would be widely up-regulated after FLV + TBI-treatment.

3.2. SCID mice and ATM knockout mice with the C3H background are refractory to the apoptosis enhanced by FLV + TBI treatment

To investigate the role of upstream molecules of p53, PI3 kinases, in FLV + TBI treatment, DNA-PK-deficient SCID mice and *ATM* knockout mice with the C3H background were analyzed. First, apoptotic cells of the bone marrow were identified using the TUNEL method (Fig. 2A). When mice were treated with TBI alone, apoptotic cells were more significantly frequent in the bone marrow of C3H·SCID (9.5 ± 0.9%, mean ± S.E.M.) than wild type C3H (6.1 ± 0.7%) at 3 h ($p < 0.01$, Student's *t*-test). These findings were consistent with the previous findings that SCID mice and cells are hypersensitive to ionizing irradiation [17]. Conversely, bone marrow cells of C3H $ATM^{-/-}$ mice exhibited significantly lower percentages of apoptotic cells (2.8 ± 0.2%) than those of wild type C3H mice ($p < 0.001$). In wild type C3H mice, apoptotic bone marrow cells were much more frequent in FLV + TBI-treated mice as compared with TBI-treated mice (Fig. 2A). Although the data are not shown, apoptotic cells before 3 h after FLV + TBI were fewer than those at 3 h. Thus, the peak apoptosis was observed at 3 h after FLV + TBI-treatment. However, in C3H·SCID and $ATM^{-/-}$ mice, the frequency of apoptotic cells after FLV + TBI treatment was similar to that after TBI-alone treatment. Thus, the enhancing effect of FLV infection on irradiation-induced apoptosis appeared negative in the bone marrow of C3H·SCID and $ATM^{-/-}$ mice. Although the data is not shown, gp70 protein levels of bone marrow cells were similar in wild, SCID, and $ATM^{-/-}$ mice after infection with FLV. Fig. 2B shows the actual figures of TUNEL reaction in the bone marrow of wild C3H mice with sham-treatment (a), TBI alone (b), and FLV + TBI treatment (c).

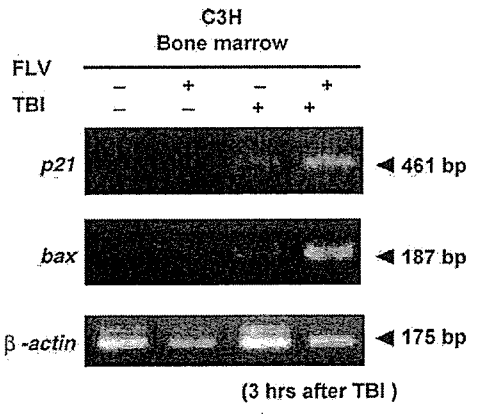

Fig. 1. RT-PCR analysis for the expression of *p21* and *bax* mRNA in the bone marrow of C3H mice. RNA samples were prepared from the bone marrow of untreated, FLV-treated, TBI-treated, and FLV + TBI-treated C3H mice 3 h after TBI treatment (+, present; –, absent). Although TBI-treatment induced a slight increase in the expression of *p21* and *bax* mRNA, FLV + TBI-treatment induced a remarkable increase of *p21* and *bax* expression.

3.3. p53 is accumulated and phosphorylated in the bone marrow of C3H mice after FLV + TBI treatment but not in SCID and ATM knockout mice

Next, bone marrow cell lysate was immunoprecipitated with anti-p53 antibody and then, the precipitate was analyzed for p53 phosphorylated at Ser-18 by immunoblotting. As shown in Fig. 3, TBI-treated mice exhibited a slight increase in intensity of the phosphorylated p53 signal 3 h after TBI with a return to the control level by 12 h. By contrast, phosphorylation was prominent in bone marrow cells from FLV + TBI-treated C3H mice 3 and 12 h after TBI. Although FLV-infection alone caused weak signals of p53 accumulation and phosphorylation (FLV (+), 0 h), this may be associated with the fact that retroviral integration to the host DNA would be recognized as a mild DNA damage by the host cells [38]. Concerning the discrepancy between the timing of apoptosis as measured by TUNEL assay and the activation of the p53 pathway in FLV + TBI-treated C3H mice, several comments may have to be added. Although we could observe the peak of apoptosis at 3 h after FLV + TBI, the reaction might actually continue even after this period. Because the macrophage-lineage cells should be activated and eliminate these apoptotic cells thereafter by phagocytosis and thus, the number of apoptotic figures may represent the balance of apoptosis and the activity of cells with phagocytosis. We might be able to detect the increased or peak apoptosis before the activation of macrophage-lineage cells occur. Therefore, we might detect the p53 activation still at 12 h after FLV + TBI. Actual apoptosis may continuously be induced because the in vivo experiments revealed remarkable loss of bone marrow hematopoietic cells in due course resulting in almost depletion by 20 days after FLV + TBI treatment.

As shown in Fig. 3, bone marrow cells of TBI-treated SCID mice exhibited p53 accumulation and phosphoryla-

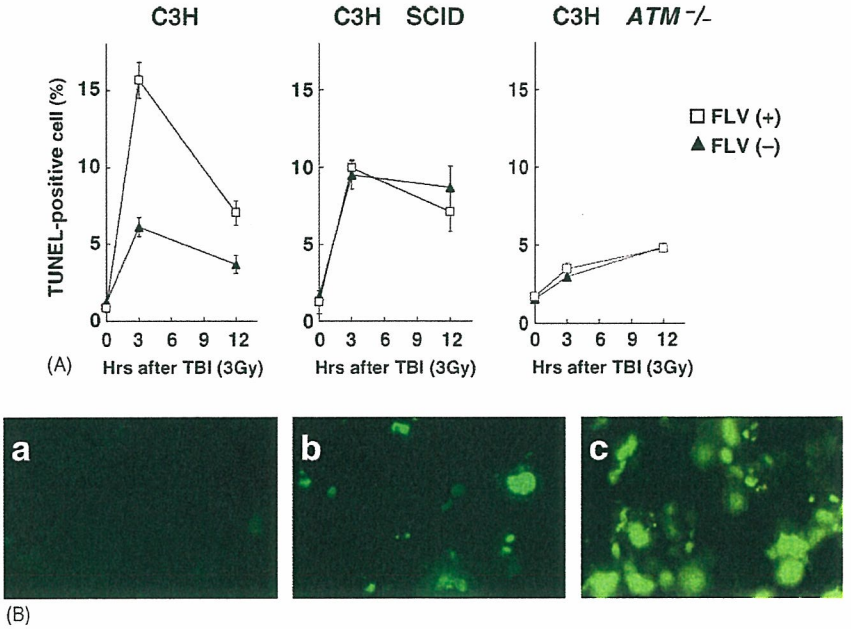

Fig. 2. (A) Apoptotic cell ratio and p53 status in the bone marrow of wild type, SCID, and $ATM^{-/-}$ mice with the C3H background after treatment with FLV and/or TBI. The TUNEL-positive cell ratio of bone marrow cells from FLV (−) or FLV (+) C3H wild type, C3H·SCID, and C3H·$ATM^{-/-}$ mice after treatment with TBI (3 Gy). Error bars indicate standard errors of the means calculated from the data from three to five mice at each point. C3H wild type mice exhibited a prominent increase in the ratio of TUNEL-positive cells with a peak at 3 h after TBI treatment, however in SCID and $ATM^{-/-}$ mice, the frequency of TUNEL-positive cells in FLV-infected mice was similar to that in FLV (−) mice after TBI treatment. (B) Apoptotic cells in the bone marrow of TBI-treated or FLV + TBI-treated mice with the C3H background. TUNEL staining of bone marrow specimens from a sham-treated control mouse (a), TBI-treated mouse (b), and FLV + TBI-treated mouse (c). Bone marrow samples were isolated at 3 h after TBI (3 Gy)-treatment and stained for apoptotic cells (original magnification, 130×). Note the many TUNEL-positive cells in the FLV + TBI-treated C3H mouse in contrast to the TBI alone-treated mouse.

tion, whereas TBI-treated $ATM^{-/-}$ mice showed almost no signal for p53 and phospho-p53 protein. After FLV + TBI-treatment, the expression of p53 and phospho-p53 protein did not show a remarkable increase in the bone marrow cells of either mice. These results indicated that ATM was required for the activation of p53 in response to TBI alone, but DNA-PK as well as ATM was required for enhanced p53 activation in C3H bone marrow cells after treatment with FLV + TBI.

3.4. DNA-PK is overexpressed after treatment with FLV + TBI

To determine the expression dynamics of DNA-PK and ATM after TBI treatment at the protein level, immunoblotting was performed using whole lysate from C3H bone marrow cells. In FLV-free (−) mice, DNA-PK expression seemed stable after TBI treatment, however, FLV-infected (+) mice exhibited a prominent increase of DNA-PK expression after the treatment (Fig. 4A). In contrast, the expression of ATM was slightly up-regulated both in FLV (−) and FLV (+) mice peaking at 3 h after TBI, although the pattern of dynamics and the intensity of bands were similar in the FLV (−) and FLV (+) conditions. ATM usually introduces *p53*-dependent apoptosis after TBI treatment. We interpreted the role of ATM in FLV + TBI-treatment as the trigger for elevating the basic level of p53-activation by TBI. Therefore, the kinetics of ATM protein expression appeared equivalent in mice regardless of FLV infection. In contrast, DNA-PK may not be essential for DNA-damage-induced apoptosis itself because SCID mice exhibited certain level of apoptosis after TBI-treatment as shown in Fig. 2A, but would be important for additional activation of p53 by FLV-infection.

Next, to test whether the overexpression of DNA-PK protein is correlated with the expression at the mRNA level, RT-PCR assays were performed for *DNA-PK* and *ATM* mRNA in each experimental group. As shown in Fig. 4B, the mRNA expression of *DNA-PK* and *ATM* appeared rather stable after treatment with FLV, TBI or FLV + TBI, although *ATM* expression was slightly enhanced by FLV-infection. These results in Fig. 4A and B suggested that mechanisms such as post-transcriptional regulation might control the protein levels of these PI3 kinases in TBI- or FLV + TBI-treated mice. Further study should clarify the discrepancy of *DNA-PK/ATM* expression at the protein level and the mRNA level.

3.5. DNA-PK and ATM demonstrate enhanced kinase activity after treatment with FLV + TBI

To confirm whether DNA-PK or ATM in the bone marrow cells of C3H mice treated with FLV + TBI actually

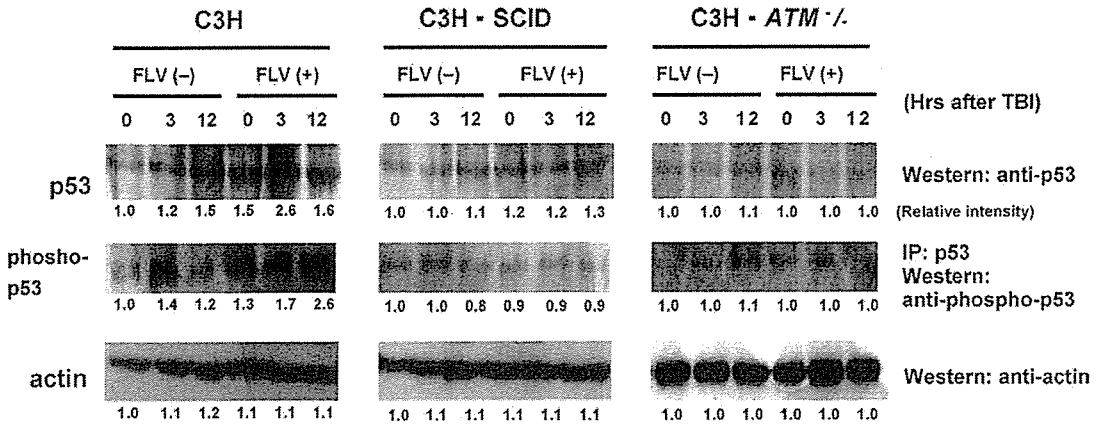

Fig. 3. Immunoblotting for p53 protein and phospho-p53 protein in bone marrow from C3H wild type, C3H·SCID, and C3H·$ATM^{-/-}$ mice 0, 3, and 12 h after TBI treatment (3 Gy). Cell lysates were prepared from the bone marrow of FLV (–) or FLV (+) C3H wild type, C3H·SCID, and C3H·$ATM^{-/-}$ mice. As the bands for actin protein exhibited a similar density in each sample, the amount of protein contained in cell lysates is similar in each lane. The relative intensities of bands were measured by densitometry (FLV (–), 0 h as the control, 1.0) and indicated under the photos of gels. C3H wild type mice revealed marked overexpression of p53 protein as well as phopspho-p53 when treated with FLV + TBI, although TBI alone also induced a slight increase of p53 and phopspho-p53 expression. By contrast, SCID and $ATM^{-/-}$ mice exhibited similar levels of p53 protein and phospho-p53 protein expression in the bone marrow samples of FLV (–) mice and FLV (+) mice after TBI-treatment.

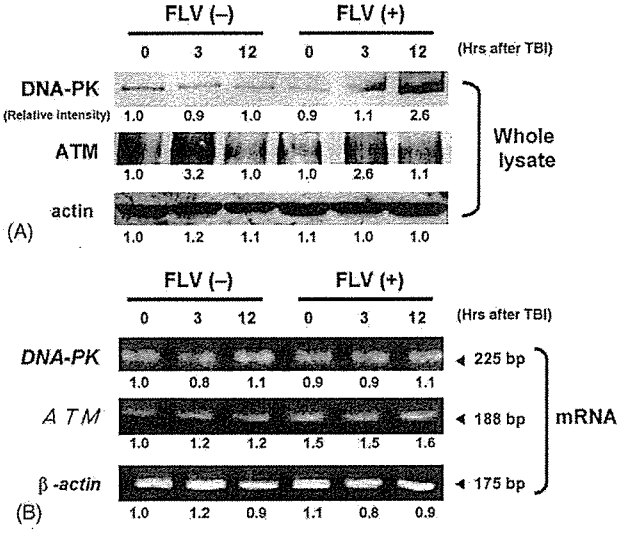

Fig. 4. (A) Immunoblotting for DNA-PK and ATM protein in the bone marrow of C3H mice 0, 3, and 12 h after TBI (3 Gy). Cell lysate (100 μg) from the bone marrow of FLV (–) or FLV (+) C3H mice was used for this assay. Actin protein levels of each sample are shown to confirm that the amounts of samples loaded were almost equal. The relative intensities of bands were measured by densitometry (FLV (–), 0 h as the control, 1.0) and indicated under the photos of gels. Note that DNA-PK protein levels were remarkably higher in the bone marrow from FLV (+) C3H mice 3 and 12 h after TBI than the FLV-treated (0 h) mice. By contrast, DNA-PK protein levels of FLV (–) C3H samples exhibited no remarkable change. ATM protein levels were enhanced by TBI-treatment but not enhanced by FLV-infection. (B) RT-PCR analysis for mRNA of *DNA-PK* and *ATM* in the bone marrow of C3H mice 0, 3, and 12 h after TBI treatment (3 Gy). The expression of *β-actin* mRNA levels of each sample was similar. The relative intensities of bands were measured by densitometry (FLV (–), 0 h as the control, 1.0) and indicated under the photos of gels. Note that changes in mRNA expression for *DNA-PK* as well as *ATM* were not remarkable between samples from each group although *ATM* expression exhibited slight increase in FLV (+) samples.

phosphorylated the p53 protein, kinase assays of DNA-PK and ATM were performed using bone marrow cells of FLV (–) and FLV (+) C3H mice treated with TBI. As DNA-PK and ATM can phosphorylate Ser-15 of p53 protein in vitro [10,12,13,39], immunoprecipitates obtained with anti-DNA-PK or anti-ATM antibody using protein extracts of bone marrow cells were mixed with exogeneous p53 protein as the substrate. Then, the phosphorylation of p53 was determined by immunoblotting with anti-phospho-p53 Ser-15 antibody (also reacted with murine Ser-18 of phospho-p53) to evaluate the DNA-PK/ATM kinase activity (Fig. 5). The differences in p53 phosphorylation levels may probably be influenced by the unequal presence of immunoprecipitated kinases (DNA-PK or ATM) as shown in Fig. 4A.

The DNA-PK activity was at the control level after treatment with TBI alone, while FLV + TBI evoked a high level of DNA-PK activity in C3H mice. In the ATM kinase assay, the phospho-p53 band exhibited a higher level in mice treated with TBI alone than in control mice. Further, the ATM kinase activity of bone marrow cells from FLV + TBI-treated C3H mice was only slightly stronger than that of TBI-treated mice. Both of DNA-PK and ATM kinase activities were slightly up-regulate by FLV alone-treatment (FLV (+), 0 h). These signals might correspond to the mild DNA damage signals by retroviral integration to the host cells [38]. As negative controls, immunoprecipitates obtained with anti-DNA-PK or anti-ATM antibody that were not mixed with exogenous p53 protein were also examined for Ser-18 phospho-p53 and exhibited negative signals (data not shown). These results suggested that TBI-treatment activated ATM kinase but not DNA-PK, although FLV + TBI treatment enhanced the ability of DNA-PK in addition to the ATM kinase to activate p53.

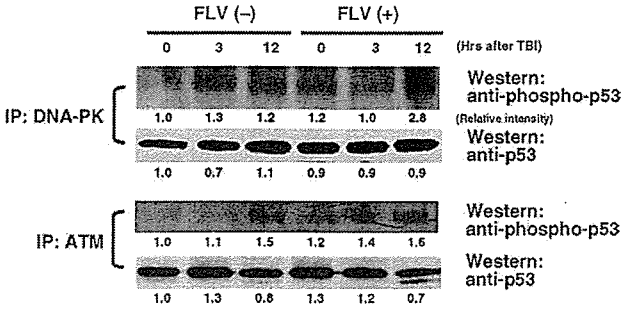

Fig. 5. Kinase assays for DNA-PK and ATM from the bone marrow of C3H mice 0, 3, and 12 h after TBI (3 Gy). Cell extracts were prepared from the bone marrow of FLV (–) or FLV (+) C3H mice. Immunoprecipitates for DNA-PK or ATM were prepared by mixing equal amount of lysate with anti-DNA-PK or ATM antibody. The kinase activity of each immunoprecipitate which would phosphorylate recombinant human p53 protein at Ser 15 in vitro was assessed by immunoblotting for phospho-p53 protein. The relative intensities of bands were measured by densitometry (FLV (–), 0 h as the control, 1.0) and indicated under the photos of gels. The same samples after the kinase reaction were also assayed for the amount of total p53 protein by immunoblotting. Note the prominent signals for phospho-p53 in FLV + TBI-treated mice at 12 h in the DNA-PK immunoprecipitate. By contrast, ATM immunoprecipitates from FLV (–) and FLV (+) mice exhibited a similar enhancement of phospho-p53 signals at 12 h after TBI, although FLV (+) mice exhibited a little stronger signal than FLV (–) mice. The total amount of p53 protein in the DNA-PK immunoprecipitates and ATM immunoprecipitates was similar in each experimental group.

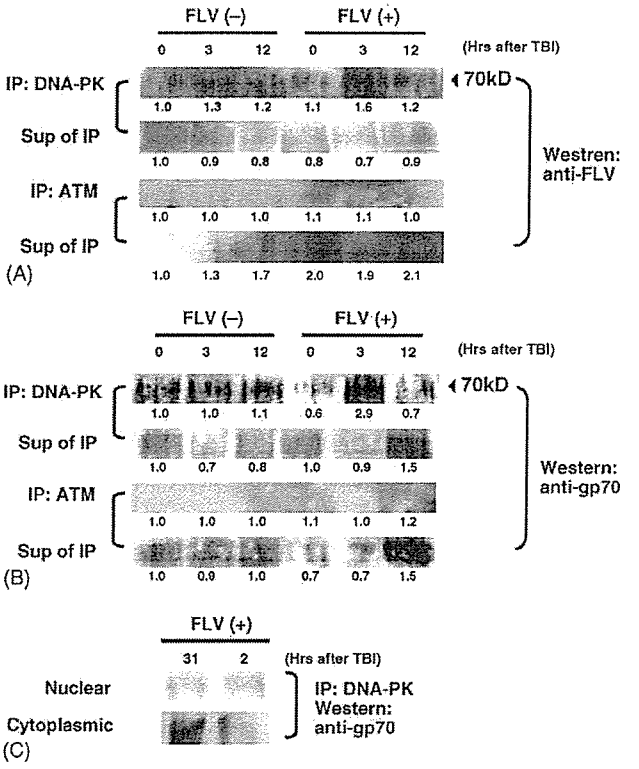

Fig. 6. (A) Co-immunoprecipitation analysis for DNA-PK or ATM with FLV-associated protein detected by anti-Friend MuLV antibody in the bone marrow of C3H mice 0, 3, and 12 h after TBI treatment (3 Gy). Cell lysate from bone marrow of FLV (–) or FLV (+) C3H mice was immunoprecipitated with anti-DNA-PK or anti-ATM antibody, then the immunoprecipitates were immunoblotted using antibody against Friend MuLV which is known to cross-react with FLV-associated proteins. Supernatants of the immnoprecipitates were also immunoblotted for FLV-associated proteins. The FLV-associated proteins were strongly co-immunoprecipitated with DNA-PK in the bone marrow of FLV (+) C3H mice 3 h after TBI at the size circa 70 kD, whereas no co-immunoprecipitation of viral protein with ATM was detected in any samples. Although the viral protein was also detected in FLV (–) mice, these weak signals would indicate the cross-reaction of this antibody with endogenous viral proteins. (B) A similar experiment using anti-Moloney MuLV gp70 antibody which is known to cross-react with Friend MuLV gp70. Note that gp70 was strongly co-immunoprecipitated with DNA-PK in the bone marrow of FLV + TBI-treated C3H mice. The relative intensities of bands were measured by densitometry (FLV (–), 0 h as the control, 1.0) and indicated under the photos of gels. (C) Co-immunoprecipitation analysis for DNA-PK with gp70 using fractionated cell lysate of the bone marrow from FLV-infected C3H mice 3 and 12 h after TBI treatment (3 Gy). Nuclear fraction and cytoplasmic fraction of cell lysate were prepared from FLV + TBI-treated mice and then, the immunoprecipitates with anti-DNA-PK antibody were immunoblotted using antibody against Moloney MuLV gp70. Note the positive signals in the cytoplasmic fraction of lysate from FLV + TBI-treated mice.

3.6. DNA-PK interacts with gp70 in response to FLV + TBI-treatment

As FLV enhances apoptosis and p53 activation in DNA damage-induced signaling pathways, an FLV-specific molecule might be involved in the activation of p53. Thus, to examine the interactions between p53 protein, DNA-PK, ATM, and the FLV-specific molecule, lysates from C3H bone marrow cells were immunoprecipitated with anti-DNA-PK or anti-ATM antibody and then, the precipitates were immunoblotted for FLV-associated proteins using polyclonal antibody against FLV-associated proteins. As shown in Fig. 6A, protein with circa 70 kD size appeared strongly co-precipitated with DNA-PK in the bone marrow cells of FLV-infected C3H mice (3 h after TBI treatment). When supernatants of DNA-PK immunoprecipitates were immunoblotted for FLV-associated proteins, we could confirm that bands for the same protein (about 70 kD in size) were relatively stronger in samples 0 and 12 h after TBI than in the sample 3 h after TBI. In contrast, immunoprecipitates obtained with anti-ATM antibody did not exhibit any positive bands for FLV-associated proteins (Fig. 6A). Because we could detect the viral protein with the molecular size around 70 kD, further to confirm the specificity of interaction of DNA-PK with gp70, which is known as a F-MuLV env protein [40], similar experiments were performed using anti-Moloney MuLV gp70 antibody and anti-Raucher MuLV gp70 antibody. As shown in Fig. 6B (only the Moloney MuLV gp70 data are shown because the data were basically identical), viral protein with the molecular size of about 70 kD was co-precipitated with DNA-PK but not with ATM in FLV + TBI-treated mice, although it is still unclear whether the interaction was direct or indirect. Taken together with the data from Fig. 4A, DNA-PK was accumulated (peaked at 12 h) after strong interaction with gp70 (peaked at 3 h) in FLV + TBI-treated C3H bone marrow cells. These findings would suggest that

the increase in the amount of DNA-PK might be related to the interaction between DNA-PK and gp70. Co-precipitation was not demonstrated between p53 and DNA-PK, p53 and ATM, or p53 and gp70 (data not shown). To determine whether the interaction occur in the cytoplasm or nucleus of FLV-infected cells, fractionated lysate was analyzed for co-precipitation of gp70 with DNA-PK. As shown in Fig. 6C, gp70 was mainly co-precipitated with DNA-PK in the cytoplasmic fraction of cell lysate from FLV + TBI treated mice.

4. Discussion

Ionizing irradiation induces a marked increase in cellular p53 protein followed by the consequent transmission of DNA damage signals [1]. The prominent apoptosis induced by FLV + TBI-treatment in the present study was *p53*-dependent, although the apoptosis observed in liquid-cultured FLV-induced primary erythroleukemic cells has been reported to be *p53*-independent [41]. As expected, expression of the *p53* target molecule, *bax*, was up-regulated, however, *p21* which has a role in cell cycle arrest signaling was also overexpressed. These findings suggested that FLV + TBI treatment induced p53 activation leading to not only apoptosis but also other DNA damage responses. Therefore, key molecules modifying the transcriptional activity of *p53* might be located upstream of p53 in the signaling pathway of this model.

In response to DNA-double strand breaks, candidates for the upstream activators of p53 would include two members of the PI3 kinase family, ATM and DNA-PK. ATM phosphorylates p53 in vivo [13], while DNA-PK has been proved to phosphorylate p53 in in vitro systems but not in in vivo systems [9]. Using mouse embryonic fibroblasts lacking DNA-PK, Jimenez et al. [15] have demonstrated that DNA-PK was not required for the p53-dependent response to DNA damage. However, our results demonstrated that not only ATM but also DNA-PK played an important role in inducing a lethal apoptosis in FLV + TBI-treated mice in vivo, whereas only ATM but not DNA-PK was required for the mild apoptotic response after low-dose TBI in bone marrow cells of C3H mice. The result suggested that FLV infection modifies the innate signaling pathway of C3H bone marrow cells to activate p53 after irradiation.

We report here that FLV-infection actually modifies the DNA-PK molecule after treatment with TBI. gp70, known as an env protein of F-MuLV, strongly interacted with DNA-PK. The interaction was mainly observed in the cytoplasmic fraction of FLV-infected cell lysate suggesting that DNA-PK with gp70 complex would be formed in the cytoplasm and then, function as a kinase and activate *p53* signaling. DNA-PK is known to associate with various proteins including Ku, which stimulates the catalytic subunit of DNA-PK (DNA-PKcs) leading to effective V(D)J recombination and DNA double-strand break repair in vivo [17,42]. Although other factors would be involved in the interaction between DNA-PK and gp70, gp70 might act as an enhancing factor for DNA-PK to be immediately accumulated and also in kinase activity to phosphorylate p53.

It remains unclear how DNA-PK or ATM works in DNA damage-induced signaling to activate p53 in FLV-infected C3H cells. Shangary et al. [37] demonstrated that ATM activated c-Abl kinase in response to ionizing irradiation and subsequently the activated c-Abl regulated DNA-PK activity in vivo. Thus, in the present experimental system also, DNA-PK and ATM might cooperate through other factors such as c-Abl kinase. Another possibility would be that DNA-PK and ATM separately activate p53 protein on FLV + TBI-treatment. The functional complementation of these two molecules was demonstrated by the fact that mice deficient in both DNA-PK (SCID mutation) and ATM show embryonic lethality [43]. In addition, the function of DNA-PK in non-homologous end joining (NHEJ) would partly be performed by ATM [38,44]. These results suggest that DNA-PK and ATM should have similar and sometimes complementary roles in various cellular pathways.

Recently, Woo et al. [45] have shown that DNA-PKcs forms a complex with latent p53 immediately following γ-irradiation, and latent murine p53 phosphorylated at Ser-18 by DNA-PK is required for DNA damage-induced apoptosis. In our experimental system, bone marrow cells from C3H·SCID mice exhibited positive signals for p53 activation and an apoptotic response when treated with TBI alone, but did not exhibit enhanced signals when treated with FLV + TBI. Thus, DNA-PK is not required for DNA damage-induced apoptosis, although signaling modulation by FLV infection would cause DNA-PK participation in apoptosis in response to DNA damage. Therefore, our present data would indicate the existence of some unidentified factor(s) amplifying mild DNA damage signals to induce severe cell death. Molecules involved in the DNA-PK-gp70 association or in the overexpression of DNA-PK might be the key to clarifying these mechanisms.

Controlling p53-mediated apoptosis would be one of the most attractive strategies of gene therapy for cancer [46]. The modifier of p53 for strong activation would be crucial to make the *p53*-gene therapy more effective. The mechanism of DNA-PK-associated p53 signaling modification leading to enhanced apoptosis should be clarified not only to understand the complexity of p53 signaling changed by retroviral infection but also to effectively use the p53 function in gene therapy aimed at cancer.

Acknowledgements

This work was supported in part by Research Grants from the National Institute of Radiological Sciences, Chiba, Japan and by a Grant-in-Aid from the Ministry of Education, Culture, Sports, Science and Technology of Japan.

References

[1] Ko LJ, Prives C. p53: puzzle and paradigm. Genes Dev 1996;10:1054–72.
[2] Levine AJ. p53, the cellular gatekeeper for growth and division. Cell 1997;88:323–31.
[3] Vogelstein B, Lane D, Levine AJ. Surfing the p53 network. Nature 2000;408:307–10.
[4] Chehab NH, Malikzay A, Stavridi ES, Harazonetis TD. Phosphorylation of Ser-20 mediates stabilization of human p53 in response to DNA damage. Proc Natl Acad Sci USA 1999;96:13777–82.
[5] Shieh SY, Ikeda M, Taya Y, Prives C. DNA damage-induced phosphorylation of p53 alleviates inhibition by MDM2. Cell 1997;91:325–34.
[6] Barlow C, Brown KD, Deng CX, Tagle DA, Wynshaw-Boris A. ATM selectively regulates distinct p53-dependent cell-cycle checkpoint and apoptotic pathways. Nature Genet 1997;17:453–6.
[7] Woo RA, McLure KG, Lees-Miller SP, Rancourt D, Lee PWK. DNA-dependent protein kinase acts upstream of p53 in response to DNA damage. Nature 1998;394:700–4.
[8] Wang S, Guo M, Ouyang H, Li X, Cordon-Cardo C, Kurimasa A, et al. The catalytic subunit of DNA-dependent protein kinase selectively regulates p53-dependent apoptosis but not cell-cycle arrest. Proc Natl Acad Sci USA 2000;97:1584–8.
[9] Araki R, Fukumura R, Fujimori A, Taya Y, Shiloh Y, Kurimasa A, et al. Enhanced phosphorylation of p53 Serine 18 following DNA damage in DNA-dependent protein kinase catalytic subunit-deficient cells. Cancer Res 1999;59:3543–6.
[10] Banin S, Moyal S, Shieh SY, Taya Y, Anderson CW, Chessa L, et al. Enhanced phosphorylation of p53 by ATM in response to DNA damage. Science 1998;281:1674–7.
[11] Burma S, Kurimasa A, Xie G, Taya Y, Araki R, Abe M, et al. DNA-dependent protein kinase-independent activation of p53 in response to DNA damage. J Biol Chem 1999;274:17139–43.
[12] Cannan CE, Lim DS. The role of ATM in DNA damage responses and cancer. Oncogene 1998;17:3301–8.
[13] Cannan CE, Lim DS, Cimprich KA, Taya Y, Tamai K, Sakaguchi K, et al. Activation of the ATM kinase by ionizing radiation and phosphorylation of p53. Science 1998;281:1677–9.
[14] Jhappan C, Yusufzai TM, Anderson S, Anver MR, Melino G. The p53 response to DNA damage in vivo is independent of DNA-dependent protein kinase. Mol Cell Biol 2000;20:4075–85.
[15] Jimenez GS, Bryntesson F, Torres-Arzayus MI, Priestley A, Beeche M, Saito S, et al. DNA-dependent protein kinase is not required for the p53-dependent response to DNA damage. Nature 1999;400:81–3.
[16] Durocher D, Jackson SP. DNA-PK, ATM and ATR as sensors of DNA damage: variations on a theme? Curr Opin Cell Biol 2001;13:225–31.
[17] Smith GCM, Jackson SP. The DNA-dependent protein kinase. Genes Dev 1999;13:916–34.
[18] Thome M, Schneider P, Hofmann K, Fickenscher H, Meinl E, Neipel F, et al. Viral FLICE-inhibitory proteins (FLIPs) prevent apoptosis induced by death receptors. Nature 1997;386:517–21.
[19] Sevilla L, Aperlo C, Dulic V, Chambard JC, Boutonnet C, Pasquier O, et al. The ets2 transcription factor inhibits apoptosis induced by colony-stimulating factor 1 deprivation of macrophages through a bcl-xL-dependent mechanism. Mol Cell Biol 1999;19:2624–34.
[20] Badley AD, Pilon AA, Landay A, Lynch LH. Mechanisms of HIV-associated lymphocytic apoptosis. Blood 2000;96:2951–64.
[21] Bonzon C, Fan H. Moloney murine leukemia virus-induced preleukemic thymic atrophy and enhanced thymocyte apoptosis correlate with disease pathogenicity. J Virol 1999;73:2434–41.
[22] Hollesberg P. Mechanisms of T-cell activation by human T-cell lymphotropic virus type I. Microbiol Mol Biol Rev 1999;63:308–33.
[23] Kitagawa M, Yamaguchi S, Hasegawa M, Tanaka K, Sado T, Hirokawa K, et al. Friend leukemia virus infection enhances DNA damage-induced apoptosis of hematopoietic cells, causing lethal anemia in C3H hosts. J Virol 2002;76:7790–8.
[24] Kelley LL, Hicks GG, Hsieh FF, Prasher JM, Green WF, Miller MD, et al. Endogenous p53 regulation and function in early stage Friend virus-induced tumor progression differs from that following DNA damage. Oncogene 1998;17:1119–30.
[25] Quang CT, Wessely O, Pironin M, Beug H, Ghysdael J. Cooperation of Spi-1/PU.1 with an activated erythropoietin receptor inhibits apoptosis and Epo-dependent differentiation in primary erythroblasts and induces their Kit ligand-dependent proliferation. EMBO J 1997;16:5639–53.
[26] Pereira R, Quang CT, Lesault I, Dolznig H, Beug H, Ghysdael J. FLI-1 inhibits differentiation and induces proliferation of primary erythroblasts. Oncogene 1999;18:1597–608.
[27] Blunt T, Finnie NJ, Taccioli GE, Smith GCM, Demengeot J, Gottlieb TM, et al. Defective DNA-dependent protein kinase activity is linked to V(D)J recombination and DNA repair defects associated with the murine SCID mutation. Cell 1995;80:813–23.
[28] Kirchgessner CU, Patil CK, Evans JW, Cuomo CA, Fried LM, Carter T, et al. DNA-dependent kinase (p350) as a candidate gene for the murine SCID defect. Science 1995;267:1178–83.
[29] Peterson SR, Kurimasa A, Oshimura M, Dynan WS, Bradbury EM, Chen DJ. Loss of the catalytic subunit of the DNA-dependent protein kinase in DNA double-strand break repair mutant mammalian cells. Proc Natl Acad Sci USA 1995;92:3171–4.
[30] Barlow C, Hirotsune S, Paylor R, Liyanage M, Eckhaus M, Collins F, et al. *ATM*-deficient mice: a paradigm of ataxia telangiectasia. Cell 1996;86:159–71.
[31] Kitagawa M, Matsubara O, Kasuga T. Dynamics of lymphocytic subpopulations in Friend leukemia virus-induced leukemia. Cancer Res 1986;46:3034–9.
[32] Kitagawa M, Kamisaku H, Sado T, Kasuga T. Friend leukemia virus-induced leukemogenesis in fully H-2 incompatible C57BL/6 → C3H radiation bone marrow chimeras. Leukemia 1993;7:1041–6.
[33] Kitagawa M, Aizawa S, Kamisaku H, Hirokawa K, Ikeda H. Protection of retrovirus-induced disease by transplantation of bone marrow cells transduced with MuLV *env* gene via retrovirus vector. Exp Hematol 1999;27:234–41.
[34] Kitagawa M, Takahashi M, Yamaguchi S, Inoue M, Ogawa S, Hirokawa K, et al. Expression of inducible nitric oxide synthase (NOS) in bone marrow cells of myelodysplastic syndromes. Leukemia 1999;13:699–703.
[35] Kitagawa M, Aizawa S, Kamisaku H, Sado T, Ikeda H, Hirokawa K. Distribution of *Fv-4* resistant gene product in Friend leukemia virus-resistant *Fv-4*^{r} mouse strain. Exp Hematol 1996;24:1423–31.
[36] Dignam JD, Martin PL, Shastry BS, Roeder RG. Eukaryotic gene transcription with purified components. Methods Enzymol 1983;101:582–98.
[37] Shangary S, Brown KD, Adamson AW, Edmonson S, Ng B, Pandita TK, et al. Regulation of DNA-dependent protein kinase activity by ionizing radiation-activated Abl kinase is an ATM-dependent process. J Biol Chem 2000;275:30163–8.
[38] Daniel R, Katz RA, Skalka AM. A role for DNA-PK in retroviral DNA integration. Science 1999;284:644–7.
[39] Lees-Miller SP, Sakaguchi K, Ullrich SJ, Appella E, Anderson CW. Human DNA-activated protein kinase phosphorylates serines 15 and 37 in the amino-terminal transactivation domain of human p53. Mol Cell Biol 1992;12:5041–9.
[40] Ikeda H, Odaka T. Cellular expression of murine leukemia virus gp-70-related antigen on thymocytes of uninfected mice correlated with *Fv-4* gene-controlled resistance to Friend leukemia virus infection. Virology 1983;128:127–39.
[41] Howard J, Ung Y, Adachi D, Ben-David Y. p53-independent tumor growth and in vitro cell survival for F-MuLV-induced erythroleukemias. Cell Growth Differ 1996;7:1651–60.
[42] Jeggo PA. DNA-PK: at the cross-roads of biochemistry and genetics. Mutat Res 1997;384:1–14.

[43] Gurley KE, Kemp CJ. Synthetic lethality between mutation in ATM and DNA-PK_{CS} during murine embryogenesis. Curr Biol 2001;11:191–4.
[44] Daniel R, Katz RA, Merkel G, Hittle JC, Yen TJ, Skalka AM. Wortmanin potentiates integrase-mediated killing of lymphocytes and reduces the efficiency of stable transduction by retroviruses. Mol Cell Biol 2001;21:1164–72.
[45] Woo RA, Jack MT, Xu Y, Burma S, Chen DJ, Lee PWK. DNA damage-induced apoptosis requires the DNA-dependent protein kinase, and is mediated by the latent population of p53. EMBO J 2002;21:3000–8.
[46] McCormick F. Cancer gene therapy: fringe or cutting edge? Nat Rev Cancer 2001;1:130–41.

Available online at www.sciencedirect.com
SCIENCE DIRECT®
Leukemia Research 29 (2005) 933–942
Leukemia Research
www.elsevier.com/locate/leukres

Resistance against Friend leukemia virus-induced leukemogenesis in DNA-dependent protein kinase (DNA-PK)-deficient *scid* mice associated with defective viral integration at the *Spi-1* and *Fli-1* site

Maki Hasegawa [a], Shuichi Yamaguchi [a], Shiro Aizawa [b], Hidetoshi Ikeda [c], Kouichi Tatsumi [b], Yuko Noda [b], Katsuiku Hirokawa [a], Masanobu Kitagawa [a,*]

[a] *Department of Comprehensive Pathology, Aging and Developmental Sciences, Tokyo Medical and Dental University, Graduate School, 1-5-45 Yushima, Bunkyo-ku, Tokyo 13-8519, Japan*
[b] *Research Center for Radiation Safety, National Institute of Radiological Sciences, 4-9-1 Anagawa, Inage-ku, Chiba 263-8555, Japan*
[c] *Laboratory of Infectious Diseases, National Institute of Animal Health, 3-1-5 Kannondai, Tsukuba City, Ibaraki 305-0856, Japan*

Received 5 October 2004; accepted 22 January 2005
Available online 11 March 2005

Abstract

Retroviral DNA integration is mediated by the viral protein integrase. However, elements of the host DNA repair machinery such as the phosphatidylinositol 3-kinase (PI-3K)-related protein kinase family system would play a role in the integration of viral DNA into the host DNA. Here, we show that a host PI-3K-related protein kinase, DNA-dependent protein kinase (DNA-PK), plays a role in the specific integration of retroviral DNA and induction of retroviral diseases in vivo. DNA-PK-deficient *scid* mice inoculated with Friend leukemia virus (FLV) exhibited a random integration into their genomic DNA and expressed the viral envelope protein gp70. However, the specific integration of FLV at *Spi-1* or *Fli-1* sites did not occur in association with the significant resistance of *scid* mice to FLV-induced leukemogenesis. In contrast, the knockout of another member of the PI-3K-related protein kinase family, encoded by the *ataxia telangiectasia mutated* (*ATM*) gene, resulted in mice as sensitive to FLV-induced leukemogenesis as the wild type mice. FLV was specifically integrated into the DNA at *Spi-1* and *Fli-1* sites with significant expression of these transcription factors. These findings indicated that DNA-PK would be essential for controlling the in vivo integration of FLV at specific sites as well as the susceptibility to FLV-induced leukemogenesis.

Keywords: Retrovirus infection; Friend virus; DNA-PK; ATM; Integration

1. Introduction

Integration into the host DNA is an essential step in retroviral replication [1]. The integration of retroviral DNA is usually mediated by the viral protein integrase [2,3]. However, recent in vitro studies suggest that several host proteins also participate in the reaction. Daniel et al. [4] have reported that the integrase-mediated joining of retroviral and host DNA is recognized as damage by the host cells, and that DNA repair proteins, such as DNA-dependent protein kinase (DNA-PK), may be required to facilitate stable integration. The catalytic subunit of DNA-PK, DNA-PKcs, is a member of a family of large, presumably multifunctional, phosphatidylinositol 3-kinase (PI-3K)-related protein kinases [5,6]. DNA-PKcs is a component of the cellular, non-homologous end-joining (NHEJ) pathway and is known to be required for the repair of double-strand breaks induced by ionizing radiation and certain DNA-damaging drugs and for V(D)J recombination during the generation of immunoglobulin-producing cells [7]. The initial events in retroviral integration would be detected as DNA damage by the host cell and DNA-PK-mediated repair may be required for the completion of the integration process. Thus, DNA-PK-deficient murine *scid* cells infected with retroviruses showed a substantial reduction in retroviral DNA integration as compared with control cells because

* Corresponding author. Tel.: +81 3 5803 5399; fax: +81 3 5803 0123.
E-mail address: masa.pth2@med.tmd.ac.jp (M. Kitagawa).

0145-2126/$ – see front matter © 2005 Elsevier Ltd. All rights reserved.
doi:10.1016/j.leukres.2005.01.016

the abortive integration of retroviruses induced apoptosis [8]. However, other experiments using HIV-1-derived retroviral vectors and cultured *scid* cells revealed that DNA-PK is not required for efficient retroviral integration [9]. Thus, the roles of DNA-PK in the retroviral integration are still unclear.

The *ataxia telangiectasia mutated* (*ATM*) gene and the *ATM* and *Rad3*-related (*ATR*) gene, which also encode members of the PI-3K-related protein kinase family, play important roles in inducing cell cycle arrest in response to DNA damage and partially contribute to DNA repair. Using wortmannin (an irreversible inhibitor of PI-3K-related protein kinases including DNA-PK and ATM kinases) and a DNA-PK-deficient murine *scid* cell system, Daniel et al. [8] have shown that in the absence of DNA repair protein of the NHEJ pathway, ATM is required to allow stable retroviral integration and to avoid integrase-mediated cell killing. However, recent in vitro experiments using caffeine (an efficient inhibitor of ATM and ATR) and an ATM-deficient cell system demonstrated that ATR kinase activity was required for successful completion of the integration [10]. Thus, the identity and mechanism of action of proteins responsible for repair of the viral–host DNA in the retroviral integration process have differed among the experimental systems employed.

To clarify the overall contribution of PI-3K-related protein kinases to the retroviral integration process and their significance for retrovirus-induced pathogenesis, it is important to trace the overall process of retroviral infection in the in vivo system using PI-3K-related protein kinase-deficient hosts. Thus, in the present study, Friend leukemia virus (FLV) was introduced into DNA-PK-deficient *scid* mice and *ATM* knockout (−/−) mice with the C3H background although regrettably, the knockout of *ATR* is embryonic lethal [11]. The FLV-induced leukemogenicity in these in vivo systems was determined and retroviral infection-related events in these PI-3K-related protein kinase-deficient mice were analyzed.

2. Materials and methods

2.1. Mice

The 8–10-week-old male C3H/He (C3H) mice were bred from our colony at the Animal Production Facility of the National Institute of Radiological Sciences in Chiba. The *scid* mice and *ATM* knockout (−/−) mice with the C3H background were also bred from our colony. Methods for the generation of knockout constructs and *ATM* −/− mice were described elsewhere [12]. The *scid* and *ATM* −/− mice with the C3H background were generated by crossing CB.17 *scid* and 129/Sv *ATM* −/− mice [13] with the C3H strain, respectively, followed by backcrossing through more than 20 generations. All mice were maintained within a barrier-sustained specific-pathogen-free (SPF) facility. All animals were reared and treated in accordance with the guidelines governing the care and use of laboratory animals at the National Institute of Radiological Sciences (approval numbers 1997-4 and 1997-17) and also the guidelines established by the Animal Experiment Committee of the Tokyo Medical and Dental University.

2.2. Viral infection and determination of leukemogenesis

An NB-tropic Friend leukemia virus complex, originally provided by Dr. C. Friend, was prepared as described earlier [14] and injected i.p. into mice at a highly leukemogenic dose of 10^4 PFU/mouse [15]. The development of leukemia was assessed using the hematocrit (Ht) value (%) and the nucleated cell count (NCC) of peripheral blood from the tail vein ($\times 10^3$/mm^3) after inoculation with FLV. One, 2, 4 and 8 weeks after the inoculation, spleen cells were collected from experimental groups of mice, stained with phycoerythrin (PE)-conjugated monoclonal anti-erythroid cells (TER119, Pharmingen, San Diego, CA, USA), and analyzed on a FACScan (Becton Dickinson Immunocytometry Systems, Mountain View, CA, USA). The TER119-positive cell parameter was calculated [16].

2.3. Southern blot hybridization

To detect the integration of proviral DNA into spleen cells from the FLV-infected mice, Southern blot hybridization was performed for FLV-specific sequences of cellular DNA [17]. Chromosomal DNA was extracted from the spleen by the phenol extraction method [18] with modifications. The DNA (10 μg) digested with restriction enzymes was fractioned by electrophoresis through 0.7% agarose gel, transferred to a Magna nylon membrane (Micron Separations Inc., Westboro, MA, USA), and hybridized to a ^{32}P-labeled *env* probe derived from a 0.8-kb *Bam*HI–*Bam*HI fragment of the Friend MuLV *env* region [19]. Southern hybridization and washing were performed according to the manufacturer's instructions (Micron Separations Inc.). Briefly, hybridization was carried out at 65 °C for 16 h in 5× SSPE, 5× Denhardt's solution, 0.5% SDS and 10 μg/ml of heat denatured salmon sperm DNA. Washing was carried out at room temperature for 10 min in 2× SSC, at 65 °C for 60 min in 2× SSC and 0.5% SDS, and then at room temperature for 10 min in 0.1× SSC. Hybridization and washing were done in rotation in a hybridization oven. Hybridization signals were detected by exposing the imaging plate of a Bio Imaging Analyzer (Fuji Bas 2000, Tokyo, Japan). Because *Hin*dIII cut the Friend MuLV sequences at two sites outside of the probe-binding portion, randomly integrated viral DNA would be detected as smears. In contrast, *Bam*HI digestion cut both ends of the probe-binding portion because the probe was designed from a *Bam*HI–*Bam*HI fragment of Friend MuLV. Therefore, *Bam*HI digestion would demonstrate integrated viral DNA.

2.4. Direct PCR for detecting specific integration of FLV at the Spi-1 or Fli-1 site

To determine the precise location and transcriptional orientation of the proviruses, we directly amplified junc-

tion fragments of proviral and host DNA using proviral primers and flanking host DNA primers. These primers were synthesized by a commercial laboratory (Invitrogen Corp., Carlsbad, CA, USA). The following pairs of primers were used: a primer from the LTR of F-MuLV, P3, *F-MuLV-P3*: GTCGCCCGGGTACCCGTATTC, and a primer from the sequence of the F-MuLV integration site of *Fli-1*, *Fli-1-Pu*: CGCTGAAGGGAAGAGCAAGAG [26], and in the same way, that of *SFFF-P3*: CACTAGAATACGAGCCACGATAAAT, and that of the SFFV integration site, *Spi-1*, *Spi-1-Pu*: CTTTCACTTGTGTAGTTGAAGATGG. High molecular weight DNAs (150 ng) were subjected to 35 cycles of PCR in a final volume of 50 μl, containing 0.2 mM of each dNTP, 1 mM $MgSO_4$, 1.0 unit of KOD-Plus-DNA polymerase (Toyobo, Osaka, Japan) and 1× PCR buffer for KOD-Plus-DNA polymerase, and 0.3 μM of each primer. PCR was performed for 35 cycles of 1 min at 94 °C, 30 s at 60 °C and 3 min at 68 °C. Aliquots of 10 μl were analyzed by electrophoresis in 1.0 or 1.5% agarose gels and visualized using ethidium bromide fluorescence. λ/*Hin*dIII–*Eco*RI-cut DNA or *ϕXHae*III-cut DNA was run in parallel as a molecular weight marker.

2.5. Reverse transcription (RT)-polymerase chain reaction (PCR) for Spi-1 or Fli-1 expression

To determine the activation of the *Spi-1* and *Fli-1* genes which is essential for the transformation of erythroid cells during the progression of FLV-induced disease [20], RT-PCR was performed in each experimental group. The RNA was extracted from the spleen and bone marrow using an RNeasy Mini Kit (Qiagen, Valencia, CA, USA) according to the manufacturer's directions. Tissue RNA (100 ng) was used as a template for the amplification reactions. Complementary (c) DNA was synthesized using Rous-associated virus reverse transcriptase (Takara Biomedicals, Kyoto, Japan). The PCR was performed as described elsewhere [21]. Oligonucleotides as specific primers for *Spi-1* and *Fli-1* were synthesized by a commercial laboratory (Life Technologies Oriental, Tokyo, Japan). As a control reaction, β-actin was also included in each run. The sequences of primers were as follows: *Spi-1*: 5′ PCR primer ATGGAAGGGTTTTCCCTCACCGCC, 3′ PCR primer CTGCACGCTCTGCAGCTCTGTGAA; *Fli-1*: 5′ PCR primer CCAGAACATGGATGGCAAGGA, 3′ PCR primer CCCAGGATCTGATAAGGATCTGGC; β-actin: 5′ PCR primer TGGAATCCTGTGGCATCCATGA, 3′ PCR primer ATCTTCATGGTGCTAGGAGCCAG. The expected sizes of the PCR products were 216 bp for *Spi-1*, 324 bp for *Fli-1* and 175 bp for β-actin. *ϕX174/Hae*III-cut DNA was run in parallel as a molecular weight marker.

2.6. Bone marrow transplantation (BMT)

To determine whether hematopoietic cells of the *scid* mice were actually refractory to FLV-induced leukemia even under conditions of normal NK-cell activity, a BMT model to rescue the FLV-infected wild type C3H host was generated. The wild type C3H mice that had a normal immune function, in other words, that did not have elevated NK-cell activity, were inoculated with FLV. One week later when FLV-induced splenomegaly was evident, mice were lethally irradiated (9.5 Gy) and transplanted with 10^6 of bone marrow cells from C3H *scid* mice. As control experiments, FLV-free C3H mice transplanted with the C3H *scid* bone marrow cells and FLV-inoculated C3H mice transplanted with the wild type C3H bone marrow cells were also generated.

2.7. Detection of apoptosis

Fresh spleen tissue was mounted in an OCT compound (Sakura, Tokyo, Japan), frozen with liquid nitrogen and cut to make 8–10 μm thick frozen sections. To identify apoptotic cells on frozen tissue sections by terminal deoxytransferase (TdT)-mediated dUTP nick end labeling (TUNEL), an in situ cell death detection kit, fluorescein (Boeringer Mannheim, Mannheim, Germany) was used as described previously [22]. Briefly, frozen sections were fixed with a 4% paraformaldehyde solution for 20 min, washed with phosphate-buffered saline (PBS), incubated in 0.1% sodium citrate–0.1% Triton X-100 for 2 min, washed with PBS and then incubated with FITC-labeled dUTP and TdT at 37 °C for 60 min. Sections were then observed under a fluorescent microscope and the TUNEL-positive cell ratio was determined by dividing the number of positively stained cells by the total cell number (counting more than 1000 cells).

2.8. Western blot analysis for gp70 and p53 protein

Spleen cells from each group of mice were suspended in Iscove's modified Dulbecco's medium (IMDM, Sigma, St. Louis, CA, USA) containing 10% fetal bovine serum, at a concentration of 6×10^6 cells/tube and pelleted. Cell lysates were prepared by incubating the pellets on ice for 15 min in 1 ml of a lysis buffer containing 10 mM Tris–HCl (pH 7.5), 5 mM EDTA, 1% Nonidet P-40, 0.02% NaN_3, 1 mM phenylmethyl sulfonyl fluoride (PMSF), 0.1% aprotinin 100 μM leupeptin, and 100 μM tosyl-L-phenylalanyl chloromethyl ketone (TPCK) (Sigma). Supernatants were separated from debris by centrifugation at 12,000 rpm (9000 × *g*) for 5 min at 4 °C. Protein concentrations were determined using a Bio-Rad protein assay kit (Bio-Rad Laboratories, Hercules, CA, USA). The whole cell lysate (50 μg) was subjected to 8, 10 or 12.5% SDS-PAGE. Gels were transferred electrophoretically to nitrocellulose membranes (Schleicher and Schull, Dassel, Germany). The membranes were blocked in 10% skim milk in PBS, incubated with a goat polyclonal anti-gp70 (Quality Biotech, Camden, NJ, USA) or a mouse monoclonal antibody to P53 protein (Pab 240, Santa Cruz Biotechnology, Santa Cruz, CA, USA), and after being washed were incubated with a horseradish peroxidase-conjugated anti-

Table 1
Hematocrit (Ht) value of the peripheral blood from the wild type, *scid* and *ATM* −/− mice after inoculation with FLV

Mice	Time after inoculation with FLV				
	Control	1 Week	2 Weeks	4 Weeks	8 Weeks
C3H wild	51 ± 1.0	48 ± 1.0	38 ± 2.0	31 ± 4.3	21 ± 5.5[a]
C3H *scid*	46 ± 0.7	43 ± 1.5	41 ± 0.3	36 ± 3.8	38 ± 1.6[a,b]
C3H *ATM* −/−	45 ± 2.6	48 ± 5.0	42 ± 1.5	30 ± 1.7	23 ± 6.4[b]

Values indicate the mean ± S.D. of the Ht value (%) of peripheral blood in three to five mice from each experimental group. Note the gradual decrease in the Ht value of wild type and *ATM* −/− mice, 2 and 4 weeks after FLV inoculation, in contrast to the slight increase or normal level in the FLV-inoculated *scid* mice.
[a] Differences were significant between the C3H control and *scid* mice at 8 weeks after FLV inoculation using Student's *t*-test ($p < 0.01$).
[b] Differences were significant between the *scid* and *ATM* −/− mice at 8 weeks after FLV inoculation using Student's *t*-test ($p < 0.01$).

goat or anti-mouse IgG antibody (Dakopatts, Glostrup, Denmark). To confirm the equivalent loading of protein in each lane, membranes were blocked, incubated in polyclonal rabbit anti-actin antisera (Sigma), and after washing, incubated in horseradish peroxidase-conjugated anti-rabbit Ig antibody (Dakopatts). Bands in the washed membrane were detected with an enhanced chemiluminescence (ECL) system (Amersham Life Science, Buckinghamshire, UK) as described previously [22].

2.9. Densitometric analysis

The densities of bands were measured by densitometric analysis with an ImageQuant scanning imager (Molecular Dynamics, Sunnyvale, CA, USA). The relative intensities of the bends were calculated by comparing the density of the sample with that of the control.

3. Results

3.1. FLV-induced leukemogenesis in the scid and ATM −/− mice

First, to determine the leukemogenicity of FLV in DNA-PK-deficient *scid* mice and *ATM* −/− mice, parameters including the hematocrit (Ht) value, nucleated cell count (NCC) of peripheral blood, spleen weight and TER119-positive cell ratio of the spleen were determined after inoculation with a leukemogenic dose of FLV. As shown in Table 1, Ht values declined remarkably after FLV inoculation in the wild type and *ATM* −/− C3H mice. In contrast, the *scid* mice showed only a slight decrease in the Ht value. Regarding the NCC, spleen weight and TER119-positive cell ratio, FLV-inoculated wild type and *ATM* −/− mice showed a gradual but significant increase after the inoculation with FLV, while *scid* mice showed very slow or no remarkable change (Fig. 1). As shown in Fig. 2, all the FLV-inoculated wild type mice died from leukemia within 19 weeks and the *ATM* −/− mice within 15 weeks, while only 20% of the FLV-inoculated *scid* mice died from leukemia; the majority of mice lived for more than 24 weeks with no evidence of splenomegaly. The *ATM* −/− mice seemed more susceptible to FLV-induced leukemia than the wild type mice probably due to their immunodeficient nature [23,24]. These findings indicated that FLV inoculation induced leukemia in the wild type and *ATM* −/− mice, whereas, the *scid* mice were significantly refractory to FLV-induced leukemogenesis.

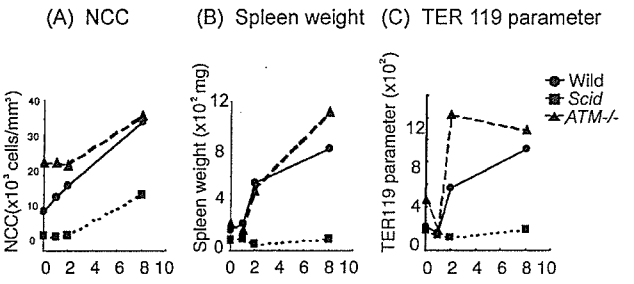

Fig. 1. FLV-induced leukemogenicity in mice with the C3H background. Lines indicate the wild type (●), *scid* (■) and *ATM* −/− mice with the C3H background (▲). Parameters for the leukemogenicity are: (A) nucleated cell count of peripheral blood ($\times 10^3$/mm^3); (B) spleen weight ($\times 10^2$ mg); (C) TER119-positive cell parameter of the spleen (spleen weight (mg) × TER119-positive cell ratio (%)/body weight (g)). Note that FLV-inoculated wild type mice and *ATM* −/− mice exhibited an increase in these parameters indicating the induction of leukemia, 4 and 8 weeks after inoculation with FLV, while *scid* mice revealed only a slight increase in each parameter.

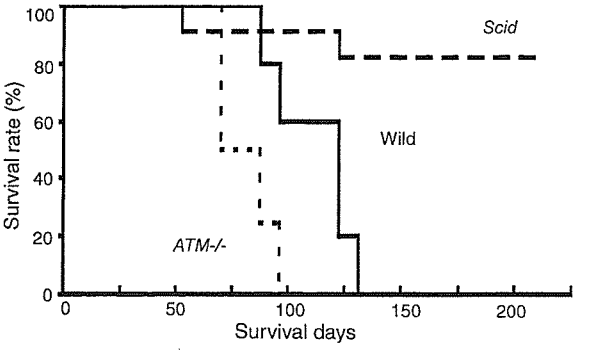

Fig. 2. Survival curves of the mice with the C3H background after inoculation with FLV. Lines indicate the wild type (solid line, $n = 10$), *scid* (broken line, $n = 13$) and *ATM* −/− (dotted line, $n = 8$) mice with the C3H background. Note the significantly longer survival of the FLV-inoculated *scid* mice compared with the FLV-inoculated wild type or *ATM* −/− mice ($p < 0.01$ and $p < 0.001$ using the Mantel–Cox test, respectively). In addition, the survival of *ATM* −/− mice was significantly shorter than that of wild type mice ($p < 0.05$).

3.2. Integration of FLV in spleen cells from the FLV-infected scid and ATM −/− mice

To investigate the actual integration of FLV into the host DNA of the *scid* and *ATM* −/− mice, Southern blot hybridization was performed to detect FLV-specific sequences in the host genome. As shown in Fig. 3A, randomly integrated FLV sequences were detected by *Hin*dIII digestion as smears, and as shown in Fig. 3B, *Bam*HI digestion demonstrated the overall integrated sequences as clear bands in spleens from the wild type and *ATM* −/− mice, 1 and 4 weeks after inoculation with FLV. Integrated signals were also clearly detected in samples from the *scid* mice, although the densities of the bands were slightly weaker. Analysis using densitometry revealed that the intensity of integration signals in *scid* mice was 2–3-fold less than those of wild mice and that the intensities in *ATM* −/− mice was almost two thirds of those of wild mice. These results suggested that the random integration of FLV did occur in the wild type and *ATM* −/− mice and also in the *scid* mice as well, although the integration efficiency seemed lower especially in *scid* mice.

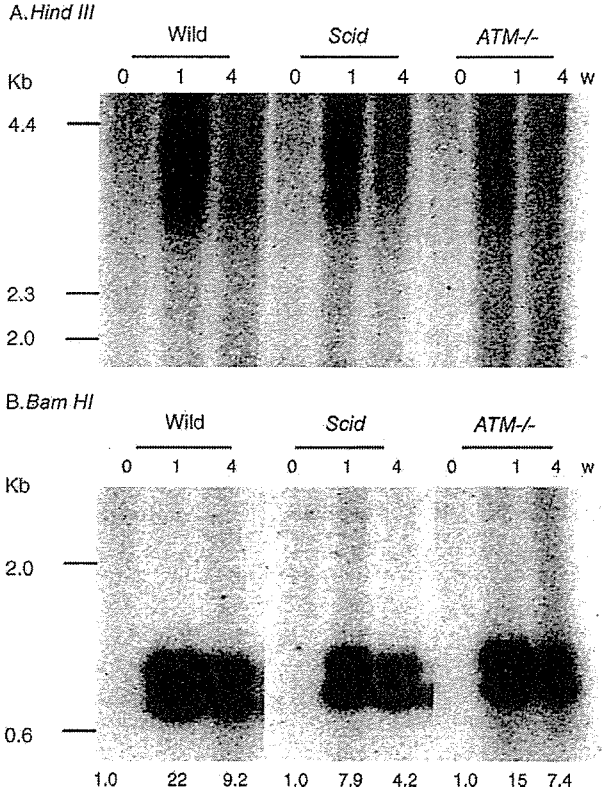

Fig. 3. Southern blot hybridization analysis for FLV-specific sequences in host DNA of the wild type, *scid* and *ATM* −/− mice after inoculation with FLV. Genomic DNA (10 μg) of high molecular weight prepared from each experimental group of mice was digested with *Hin*dIII (A) and *Bam*HI (B). Each sample was hybridized with a ^{32}P-labeled Friend MuLV-derived DNA probe. *Hin*dIII digestion was expected to detect randomly integrated F-MuLV DNA as smears and free viral cDNA as bands. In contrast, *Bam*HI digestion would reveal integrated or free DNA as distinct bands. As we could detect smear signals but not band signals in *Hin*dIII digestion experiments, free viral cDNA would be ignorable probably because we prepared the samples by a high molecular weight DNA extraction method. Note that the integrated proviral sequences of F-MuLV were prominent in the wild type and *ATM* −/− mice, 1 and 4 weeks after inoculation with FLV. The *scid* mice also demonstrated significant integration although the density of bands appeared slightly weaker. The relative intensities of bands were measured by densitometry (wild mouse sample before inoculation with FLV as the control, 1.0) and indicated under the photos of gels.

3.3. Expression of gp70 protein in spleen cells of the wild type, scid and ATM −/− mice

To confirm whether the integrated viral genes were actually expressed, the viral envelope protein gp70, was examined by Western blotting after inoculation of the wild type and *scid* mice. As shown in Fig. 4, gp70 was abundantly expressed in the spleen cells of wild type mice, 1, 4 and 8 weeks after the inoculation with FLV. In the *scid* mice also, spleen cells exhibited significant signals at 1, 4 and 8 weeks, although the expression of gp70-associated protein was observed as early as 1 and 3 days in *scid* mice. However, the overall expression of gp70 was slightly lower in the *scid* mice than the wild type mice. These findings were consistent with the data shown in Fig. 3A and B indicating the levels of FLV integration into spleen cells of the wild type and *scid* mice.

3.4. Integration of FLV at Spi-1 and Fli-1 sites and the expression of Spi-1 and Fli-1 in spleen cells of the wild type, scid and ATM −/− mice

Spi-1 and *Fli-1* are transcription factors expressed in the majority of FLV-induced leukemia cells [25,26]. Integration of the spleen focus forming virus (SFFV) occurs at the *Spi-1* site and that of the Friend murine leukemia virus (MuLV) adjacent to the *Fli-1* site. The integrated LTR of the virus promotes the expression of these transcription factors causing leukemogenesis. To detect the specific integration of viral sequences at these sites, direct PCR analysis was performed using primer sets amplifying junction fragments of the integrated viral sequences and the host transcription factor sequences. As shown in Fig. 5A, dilution experiments were performed using PCR products for the *Spi-1* site detected 1 week after inoculation with FLV and those for the *Fli-1* site by week 8 in spleen cells of the wild type mice. Both signals were evident in 5× and 1× (no dilution) samples. Then, the PCR was performed for samples from 0, 1 and 8 weeks after inoculation with FLV in wild type, *scid* and *ATM* −/− mice. As shown in Fig. 5B, PCR products for the *Spi-1* site were detected 1 week after inoculation with FLV and those for the *Fli-1* site by week 8 in spleen cells of the wild type and *ATM* −/− mice, These findings indicate that the monoclonal expansion of leukemic cells occurs with integration of SFFV at the *Spi-1* site at an early stage and later with the integration of F-MuLV at the *Fli-1* site. In contrast, spleen cells from the *scid* mice exhibited a very weak signal for *Spi-1* site integration and the undetectable level of *Fli-1* site integration signal

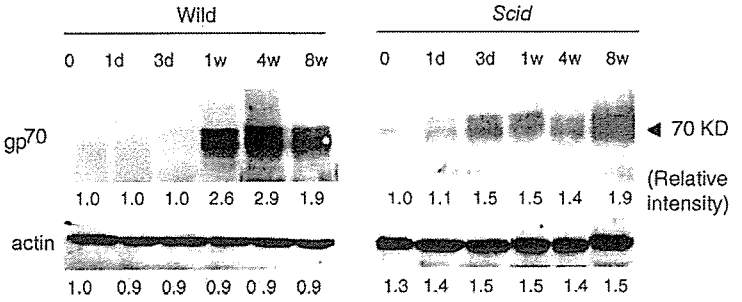

Fig. 4. Expression of gp70 in the C3H wild type and *scid* mice determined by Western blotting. The relative intensities of bands were measured by densitometry (0 day, wild type as the control, 1.0) and indicated under the photos of gels. Note that the expression of gp70 was prominent in the wild type mice, 1, 4 and 8 weeks after inoculation with FLV. The *scid* mice expressed gp70 from the earlier period after FLV inoculation (1 and 3 days) probably originated from the immunodeficient nature of these mice. In 1, 4 and 8 weeks, *scid* mice demonstrated significant expression although the density of bands in 1 and 4 weeks appeared slightly weaker than the wild type.

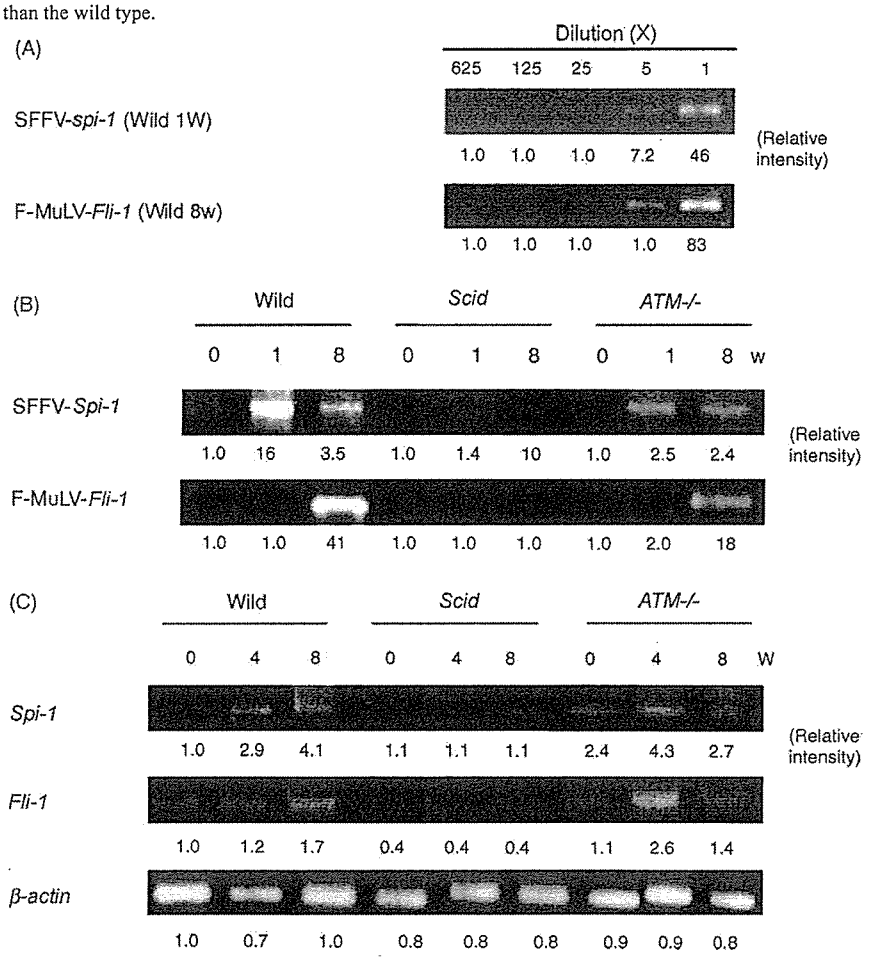

Fig. 5. Specific integration of FLV and expression of the transcription factors. Direct PCR analysis for the specific integration of FLV at the *Spi-1* or *Fli-1* site (A) and RT-PCR analysis for the mRNA expression of *Spi-1* and *Fli-1* (B) in the spleen of mice with the C3H background. DNA or RNA samples were prepared from the spleen of wild type, *scid* and *ATM* −/− mice, before and 1 and 8 weeks after inoculation with FLV. (A) DNA samples from wild type mice were prepared 1 and 8 weeks after inoculation with FLV and diluted to 5×, 25×, 125× and 625×. Direct PCR was performed for SFFV-*Spi-1* in samples from week 1 with each dilution or F-MuLV-*Fli-1* in samples from week 8. The relative intensities of bands were measured by densitometry (625× sample as the control, 1.0) and indicated under the photos of gels. Note that both signals were evident in samples 5× and 1×. (B) Direct PCR exhibited integration of SFFV at the *Spi-1* site (1 week after FLV inoculation) and F-MuLV at the *Fli-1* site (4 weeks after FLV inoculation) in spleen cells from the wild type and *ATM* −/− mice. In contrast, very weak signal was observed in spleen cells from the *scid* mice for *Spi-1* site integration and the signal was not detectable for the *Fli-1* site integration. The relative intensities of bands were measured by densitometry (0 day, wild type as the control, 1.0) and indicated under the photos of gels. (C) A RT-PCR technique revealed overexpression of mRNA for *Spi-1* and *Fli-1* in the FLV-infected wild type and *ATM* −/− samples, 4 and 8 weeks after FLV inoculation. However, up-regulation was not detectable in samples from FLV-inoculated *scid* mice. The relative intensities of bands were measured by densitometry (0 day, wild type as the control, 1.0) and indicated under the photos of gels.

suggesting that the cells with viral integration at *Spi-1* as well as *Fli-1* site did not show progressive proliferation after FLV inoculation. The defective integration of FLV to these specific sites may be related to the lower level of overall random integration in *scid* mice.

To determine whether the FLV-induced disease-specific transcription factors were activated by infection with FLV, mRNA levels of *Spi-1* and *Fli-1* was examined in spleen cells from the wild type, *scid* and *ATM* −/− mice using the RT-PCR technique. The expression of mRNA for *Spi-1* and *Fli-1* (Fig. 5C) was significantly up-regulated in FLV-inoculated wild type and *ATM* −/− mice, 4 and 8 weeks after the inoculation with FLV, as compared with the control (non-inoculated) mice. In contrast, the *scid* mice did not exhibit the expression of *Spi-1* and *Fli-1* after the inoculation. These results confirmed that FLV-infection actually evoked leukemogenesis indicated by the expression of FLV-induced disease-specific transcription factors in spleen cells of the wild type and *ATM* −/− mice but not of the *scid* mice.

3.5. Effects of scid bone marrow transplantation in the FLV-infected C3H mice

To explain the FLV-resistance of *scid* mice by the defective integration of SFFV and F-MuLV to the specific sites, several possibilities should be ruled out. One of these would be the fact that the *scid* mice have stronger NK-cell activity than wild type mice [27]. To test whether the NK cells played a role in resisting FLV-induced leukemia in the *scid* mice, we generated a *scid* bone marrow transplantation model of FLV-induced leukemogenesis. One week after inoculation with FLV, C3H wild type mice having normal NK activity were transplanted with *scid* bone marrow cells. Even under conditions where host NK-cell activity was not elevated, the transplantation effectively suppressed FLV-induced leukemogenesis as compared with the FLV-inoculated C3H mice transplanted with the wild type C3H bone marrow cells (Fig. 6). Thus, the *scid* mice might be refractory to FLV-induced leukemia not because they have strong NK-cell activity but because the *scid* cells themselves are refractory to viral integration.

3.6. Apoptosis in spleen cells of the FLV-infected scid and ATM −/− mice

The other possibility concerning the resistance of *scid* mice to FLV-induced leukemia would be the increased sensitivity to apoptosis of leukemia cells caused by DNA-PK deficiency. After retroviral infection, integrase-induced DNA breaks are known to cause apoptosis in DNA-PK-deficient *scid* cells in vitro [4]. Therefore, to estimate the apoptotic frequency in FLV-inoculated mice in vivo, spleen cells from wild type, *scid* and *ATM* −/− mice with the C3H background were subjected to the TUNEL assay. As shown in Fig. 7, the apoptotic frequency of spleen cells from the *scid* mice doubled within 12 h after the inoculation with FLV, then gradually

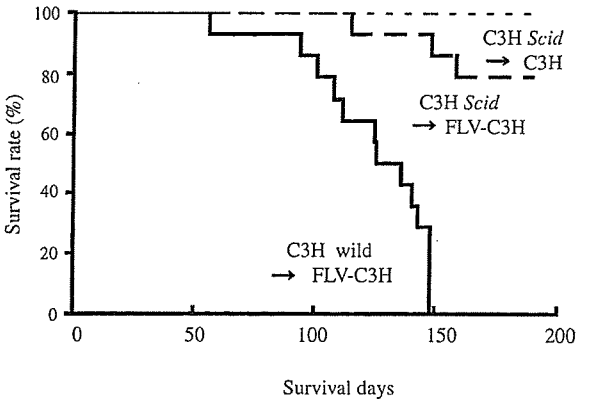

Fig. 6. Effects of *scid* bone marrow transplantation on FLV-infected wild type C3H hosts. Survival curves for C3H wild → FLV-C3H (solid line), C3H *scid* → FLV-C3H (broken line), and C3H *scid* → C3H (dotted line) demonstrating the effects of the *scid* bone marrow cell transplantation on the progression of FLV-induced leukemia. The difference was significant between the *scid* C3H → FLV-C3H and the wild C3H → FLV-C3H mice using Wilcockson's test ($p < 0.01$).

abated, returning to the normal level in 1 week. The apoptotic frequency of spleen cells from the wild type and *ATM* −/− mice did not show significant change after the inoculation. These results indicated that the hematopoietic cells of DNA-PK-deficient *scid* mice might be eliminated by apoptosis after FLV infection in part, however, the apoptotic events occurred only in the early phase of infection and further, the apoptotic cell ratio was not high enough to explain the resistance of *scid* mice to FLV-induced leukemia. Thus, the mechanism of resistance to FLV in *scid* mice appears more complicated than that in the cell culture systems.

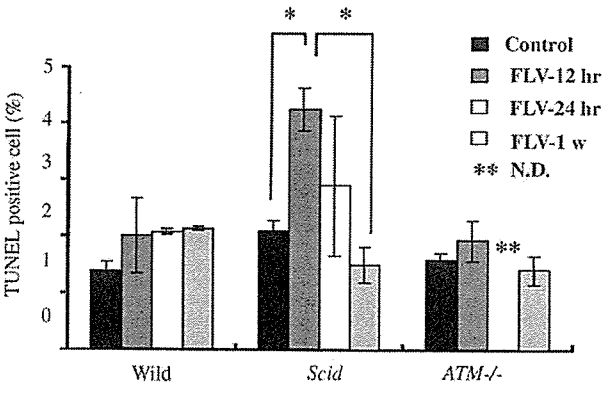

Fig. 7. TUNEL assay for detecting the frequency of apoptotic cells in spleen cells from the wild type, *scid* and *ATM* −/− mice after inoculation with FLV. Bar graphs indicate the mean value of the TUNEL-positive cell ratio (%) of bone marrow in three or four mice from each experimental group. Error bars indicate SEM. Note the remarkable increase of TUNEL-positive cells in the *scid* mice 12 h after FLV inoculation. The difference was significant between the C3H *scid* control and 12 h after FLV inoculation ($p < 0.05$) with Student's *t*-test.

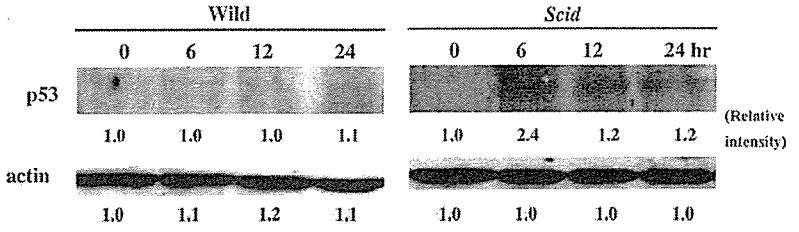

Fig. 8. Western blot analysis for the *p53* status of the FLV-inoculated wild type and *scid* mice after inoculation with FLV. Spleen cells of the wild type and *scid* mice were analyzed for the expression of P53 protein 0, 6, 12 and 24 h after inoculation with FLV. Cells were lysed and whole lysates were examined for P53 expression. The relative intensities of bands were measured by densitometry (0 day, wild type as the control, 1.0) and indicated under the photos of gels. Note the significant increase in P53 expression in the FLV-inoculated *scid* C3H mice in contrast to the almost negative signals in the wild type mice.

3.7. p53 status of the FLV-infected scid mice

p53 is known to regulate multiple cellular functions including cell cycle arrest and apoptosis. To examine whether the *p53* gene was activated in the FLV-inoculated *scid* mice, in other words, to determine whether the apoptosis that occurred in hematopoietic cells of the FLV-inoculated *scid* mice was *p53*-dependent or not, Western blot analysis was performed for P53 protein. Lysates of spleen cells from the wild type and *scid* mice were prepared 6, 12 and 24 h after inoculation with FLV. As shown in Fig. 8, the expression of P53 significantly increased in samples from the *scid* mice compared with wild type mice. Therefore, the *scid* cells might recognize FLV infection as DNA damage and overexpress P53 because of a failure to repair DNA breaks and complete the viral integration process.

4. Discussion

This study clearly demonstrates that DNA-PK-deficient *scid* mice are less susceptible to leukemia and live longer than wild type mice after infection with FLV. In consistent with the in vitro results reported by Daniel et al. [4], *scid* mouse-derived cells were certainly infected with FLV in vivo, although the integration intensity into spleen cells was lower than that in wild type mice. Our experiments revealed that the deficiency for overall integration was about 2–3-fold in *scid* mice, although Daniel et al. showed 5-fold deficiency in the in vitro system. This was consistent with the finding in vitro that DNA-PK was not essential for retroviral integration [9]. However, the most striking events in the viral integration process in *scid* mice was the defective integration of FLV at the *Spi-1* and *Fli-1* sites. As a result, overexpression of these oncogenic transcription factors did not occur in FLV-inoculated *scid* mice. These findings would suggest the significance of DNA-PK for the site-specific integration of retroviral cDNA. However, we have to remember that the defective integration of FLV to these specific sites might be influenced by the lower level of overall random integration in *scid* mice. In contrast, the *ATM* −/− mice exhibited similar changes in leukemogenesis and specific viral integration at the oncogenic transcription factor sites as the wild type mice after inoculation with FLV. These findings are consistent with in vitro data indicating that *ATM* −/− cells were susceptible to retroviral integration [4,28].

A previous study suggests that the abortive integration evoked death in the DNA repair-deficient *scid* cells in vitro [4]. In the present in vivo study also, we showed that apoptosis in hematopoietic cells was more frequent in the *scid* mice than the wild type or *ATM* −/− mice but the difference was not so marked and the change lasted only a short period after the inoculation with FLV. The resistance of *scid* mice to FLV cannot simply be explained by the promotion of apoptosis among retrovirus-infected *scid* cells.

The *ATR* gene [29], may contribute to the end-ligation reaction of DNA at the time of retroviral integration. Usually *ATR* functions in the repair of UV irradiation-induced DNA damage [30], however, we cannot ignore the possibility that this kinase may function under a NHEJ-deficient state. *ATR* overexpression can rescue some of the phenotypes of *ATM* deficiency [31]. The ATR protein phosphorylates a similar set of proteins to ATM, although the kinetics and activation signals involved seem to be different [32]. It seems likely that the specificity of the ATM and ATR reactions is determined by distinct cofactors. Thus, to clarify the function of ATR in vivo, it would be necessary to generate *DNA-PK* and *ATM* double knockout mice as well as *ATR* knockout mice, although this double knockout is known to be fatal [33,34], because the developmental arrest of embryos occurs at around E7.5, a stage when embryonic cells are hypersensitive to DNA damage [35]. Further, the knockout of *ATR* is also embryonic lethal [11].

In terms of immunological protection against FLV-induced leukemia, immunosuppressed animals were expected to be more susceptible to leukemogenesis than the immunocompetent wild type mice [14,36]. In this sense, FLV-induced leukemic cells might proliferate more easily in the immunosuppressed *scid* mice. Actually, FLV-induced disease progressed a little faster in *ATM* −/− mice which also have defects in immunological function [23,24]. Nevertheless, the *scid* mice were rather refractory to FLV-induced leukemogenesis. This may be because specific integration of FLV at the *Fli-1* site no longer occurred and the proliferation of FLV-infected cells in FLV-inoculated *scid* mice was not induced. However, the *scid* mice may have many

other characteristics including loss of mature lymphocytes and high NK-cell activity. As to the target of FLV-induced leukemogensis, the *scid* mice have enough TER119-positive cells in the spleen, although we do not know whether the signal transduction systems of the *scid* erythroid cells are completely the same as the wild type. Further, we cannot ignore the possibility that T cells or B cells might play a role in the integration/proliferation of FLV in the spleen. Although the NK-cell activity did not appear to affect FLV-resistance in the *scid* mice given the results of our BMT experiment, other possibilities should be ruled out to completely clarify the mechanism of resistance in *scid* mice. For example, we could not ignore the possibility that DNA-PK might be necessary for the clonal proliferation of FLV-induced leukemia cells in vivo.

DNA-PK is known to play an important role in the repair of double-stranded DNA breaks including the intermediate state during meiosis and the variable (diversity) joining (V(D)J) recombination by joining broken DNA molecules. However, the mechanisms for specific/non-specific recognition and ligation of blunt ends to form precise joints are still unclear. The joining of retroviral DNA integration has been shown to proceed normally in DNA-PK-deficient cells apart from a small variation in target site duplication. Furthermore, no gross abnormalities in sequence were identified at the provirus–host DNA junctions [37]. Additional experiments will be required to determine the exact role of DNA-PK and associated molecules controlling the specific integration of FLV at the *Spi-1* or *Fli-1* site.

As to the specificity of retroviral integration, the mechanism by which integration sites are chosen is not well understood, and is influenced by several factors, including DNA sequences and structure, DNA methylation and transcription. Viral integrase also plays a key role in controlling the choice of target sites. The integrase domain responsible for target site selection has been mapped to the central core region [38]. Another possible factor directing integration would be the sequence-specific DNA-binding proteins, which may fuse to integrase. Using these fusion proteins, the use of retroviral vectors could be facilitated by targeting integration in vivo at predetermined sites. However, although targeting worked well in reactions in vitro, a variety of obstacles complicated applications in vivo [39]. The present study demonstrated the novel possibility that the host enzyme, DNA-PK, controls the specificity of retroviral integration. We expect the manipulation of host gene function to also be applicable to the design of safer and more effective gene transfer systems in vivo.

Acknowledgements

This work was supported in part by a grant-in-aid for scientific research from the Ministry of Education, Culture, Sports, Science and Technology of Japan. The authors thank Prof. Tom Daniel Humphreys II, Ph.D., University of Hawaii for critical reading of the manuscript with kind and thoughtful suggestions and also for English editing.

Contributions. Maki Hasegawa contributed to the concept and design, interpreted and analyzed the data, provided drafting of the article, provided study materials/patients, and contributed to the collection and assembly of the data. Shuichi Yamaguchi contributed to the concept and design, interpreted and analyzed the data, supplied statistical expertise, and contributed to the collection and assembly of the data. Shiro Aizawa contributed to the concept and design, interpreted and analyzed the data, provided critical revisions and important intellectual content, and obtained a funding source. Hidetoshi Ikeda contributed to the concept and design, interpreted and analyzed the data, provided critical revisions and important intellectual content, and provided study materials/patients. Kouichi Tatsumi interpreted and analyzed the data, provided critical revisions and important intellectual content, and provided study materials/patients. Yuko Noda provided study materials/patients and provided administrative, technical and logistic support. Katsuiku Hirokawa provided critical revisions and important intellectual content, and provided administrative, technical and logistic support. Masanobu Kitagawa contributed to the concept and design, interpreted and analyzed the data, provided drafting of the article, gave final approval, provided study materials/patients, supplied statistical expertise, obtained a funding source, and contributed to the collection and assembly of the data.

References

[1] Katz RA, Skalka AM. The retroviral enzymes. Annu Rev Biochem 1994;63:133–73.
[2] Katz RA, Merkel G, Kulkosky J, Leis J, Skalka AM. The avian retroviral IN protein is both necessary and sufficient for integrative recombination in vitro. Cell 1990;63:87–95.
[3] Craigie R, Fujiwara T, Bushman F. The IN protein of Moloney murine leukemia virus processes the viral DNA ends and accomplishes their integration in vitro. Cell 1990;62:829–37.
[4] Daniel R, Katz RA, Skalka AM. A role for DNA-PK in retroviral DNA integration. Science 1999;284:644–7.
[5] Hartley KO, Gell D, Smith GCM, Zhang H, Divecha N, Connelly MA, et al. DNA-dependent protein kinase catalytic subunit: a relative of phosphatidylinositol 3-kinase and the ataxia telangiectasia gene product. Cell 1995;82:849–56.
[6] Keith CT, Schreiber SL. PIK-related kinases: DNA repair, recombination, and cell cycle checkpoints. Science 1995;270:50–1.
[7] Smith GCM, Jackson SP. The DNA-dependent protein kinase. Genes Dev 1999;13:916–34.
[8] Daniel R, Katz RA, Merkel G, Hittle JC, Yen TJ, Skalka AM. Wortmannin potentiates integrase-mediated killing of lymphocytes and reduces the efficiency of stable transduction by retroviruses. Mol Cell Biol 2001;21:1164–72.
[9] Baekelandt V, Claeys A, Cherepanov P, De Clercq E, De Strooper B, Nuttin B, et al. DNA-dependent protein kinase is not required for efficient lentiviral integration. J Virol 2000;74:11278–85.
[10] Daniel R, Kao G, Taganov K, Greger JG, Favorova O, Merkel G, et al. Evidence that the retroviral DNA integration process triggers an ATR-dependent DNA damage response. Proc Natl Acad Sci USA 2003;100:4778–83.

[11] Cortez D, Guntuku S, Qin J, Elledge SJ. ATR and ATRIP: partners in checkpoint signaling. Science 2001;294:1713–6.
[12] Barlow C, Hirotsune S, Paylor R, Liyanage M, Eckhaus M, Collins F, et al. *Atm*-deficient mice: a paradigm of ataxia telangiectasia. Cell 1996;86:159–71.
[13] Furuno-Fukushi I, Masumura K, Furuse T, Noda Y, Takahagi M, Saito T, et al. Effect of Atm disruption on spontaneously arising and radiation-induced deletion mutations in mouse liver. Radiat Res 2003;160:549–58.
[14] Kitagawa M, Matsubara O, Kasuga T. Dynamics of lymphocytic subpopulations in Friend leukemia virus-induced leukemia. Cancer Res 1986;46:3034–9.
[15] Kitagawa M, Aizawa S, Kamisaku H, Hirokawa K, Ikeda H. Protection of retrovirus-induced disease by transplantation of bone marrow cells transduced with MuLV *env* gene via retrovirus vector. Exp Hematol 1999;27:234–41.
[16] Yamaguchi S, Kitagawa M, Inoue M, Tejima Y, Kimura M, Aizawa S, et al. Role of lymphoid cells in age-related change of susceptibility to Friend leukemia virus-induced leukemia. Mech Ageing Dev 2001;122:219–32.
[17] Paul R, Schuetze S, Kozak SL, Kabat D. A common site for immortalizing proviral integrations in Friend erythroleukemia: molecular cloning and characterization. J Virol 1989;63:4958–61.
[18] Sambrook J, Fritsch EF, Manitais T. Molecular cloning: a laboratory manual. 2nd ed. Cold Spring Harbor, NY: Cold Spring Harbor Laboratory Press; 1989.
[19] Silver J, Kozak C. Common proviral integration region on mouse chromosome 7 in lymphomas and myelogenous leukemias induced by Friend murine leukemia virus. J Virol 1986;57:526–33.
[20] Starck J, Doubeikovski A, Sarrazin S, Gonnet C, Rao G, Skoultchi A, et al. *Spi-1*/PU.1 is a positive regulator of the *Fli-1* gene involved in inhibition of erythroid differentiation in Friend erythroleukemic cell lines. Mol Cell Biol 1999;19:121–35.
[21] Kitagawa M, Takahashi M, Yamaguchi S, Inoue M, Ogawa S, Hirokawa K, et al. Expression of inducible nitric oxide synthase (NOS) in bone marrow cells of myelodysplastic syndromes. Leukemia 1999;13:699–703.
[22] Kitagawa M, Yamaguchi S, Hasegawa M, Tanaka K, Sado T, Hirokawa K, et al. Friend leukemia virus-infection enhances DNA-damage-induced apoptosis of hematopoietic cells in C3H hosts. J Virol 2002;76:7790–8.
[23] Xu Y, Ashley T, Brainerd EE, Bronson RT, Meyn MS, Baltimore D. Targeted disruption of ATM leads to growth retardation, chromosomal fragmentation during meiosis, immune defects, and thymic lymphoma. Genes Dev 1996;10:2383–8.
[24] Chao C, Yang EM, Xu Y. Rescue of defective T cell development and function in *Atm* −/− mice by a functional TCR αβ transgene. J Immunol 2000;164:345–9.
[25] Moreau-Gachelin F, Tavitian A, Tambourin P. *Spi-1* is a putative oncogene in virally induced murine erythroleukaemias. Nature 1988;331:277–80.
[26] Sels FT, Langer S, Schulz AS, Silver J, Sitbon M, Frierich RW. Friend murine leukaemia virus is integrated at a common site in most primary spleen tumours of erythroleukaemic animals. Oncogene 1992;7:643–52.
[27] Christianson SW, Greiner DL, Schweitzer IB, Gott B, Beamer GL, Schweitzer PA, et al. Role of natural killer cells on engraftment of human lymphoid cells and on metastasis of human T-lymphoblastoid leukemia cells in C57BL/6J-*scid* mice and in C57BL/6J-*scid bg* mice. Cell Immunol 1996;171:186–99.
[28] Li L, Olivera JM, Yoden KE, Mitchell RS, Butler SL, Lieber M, et al. Role of the non-homologous DNA end joining pathway in the early steps of retroviral infection. EMBO J 2001;20:3272–81.
[29] Durocher D, Jackson SP. DNA-PK, ATM and ATR as sensors of DNA damage: variations on a theme? Curr Opin Cell Biol 2001;13:225–31.
[30] Shiloh Y. ATM and ATR: networking cellular responses to DNA damage. Curr Opin Genet Dev 2001;11:71–7.
[31] Cliby WA, Roberts CJ, Cimprich KA, Stringer CM, Lamb JR, Schreiber SL, et al. Overexpression of a kinase inactive ATR protein causes sensitivity to DNA damaging agents and defects in cell cycle checkpoints. EMBO J 1998;17:159–69.
[32] Tibbetts RS, Brumbaugh KM, Williams JM, Sarkaria JN, Cliby WA, Shieh SY, et al. A role for ATR in the DNA damage induced phosphorylation of p53. Genes Dev 1999;13:152–7.
[33] Gurley KE, Kemp CJ. Synthetic lethality between mutation in Atm and DNA-PKcs during murine embryogenesis. Curr Biol 2001;11:191–4.
[34] Sekiguchi JA, Ferguson DO, Chen HT, Yang EM, Earle J, Frank K, et al. Genetic interactions between ATM and the nonhomologous end-joining factor in genomic stability and development. Proc Natl Acad Sci USA 2001;98:3243–8.
[35] Heyer BS, MacAuley A, Behrendtsen O, Werb Z. Hypersensitivity to DNA damage leads to increased apoptosis during early mouse development. Genes Dev 2000;14:2072–84.
[36] Zhang F, Ya LT, Iwatani Y, Higo K, Suzuki T, Tanaka M, et al. Resistance to Friend murine leukemia virus infection conferred by the Fv-4 gene is recessive but appears dominant from the effect of the immune system. J Virol 2000;74:6193–7.
[37] Taganov K, Daniel R, Katz RA, Favorova O, Skalka AM. Characterization of retrovirus–host DNA junctions in cells deficient in nonhomologous-end joining. J Virol 2001;75:9549–52.
[38] Holmes-Son ML, Appa RS, Chow SA. Molecular genetics and target site specificity of retroviral integration. Adv Genet 2001;43:33–69.
[39] Bushman FD. Integration site selection by lentiviruses: biology and possible control. Curr Top Microbiol Immunol 2002;261:165–77.

ORIGINAL ARTICLE

Nestin expression in odontoblasts and odontogenic ectomesenchymal tissue of odontogenic tumours

S Fujita, K Hideshima, T Ikeda

J Clin Pathol 2006;**000**:1–7. doi: 10.1136/jcp.2004.025403

Background: Nestin, one of the intermediate filaments constituting the cytoskeleton, is a marker of neural stem cells or progenitor cells. Its expression is also related to tooth development and repair of dentine.
Aims: The aim of this study was to investigate nestin expression in various odontogenic tumours and evaluate its usefulness for histopathological diagnosis.
Methods: We studied formalin fixed, paraffin embedded specimens from 129 cases of odontogenic tumours and 9 of mandibular intraosseous myxoma. After characterisation of odontogenic ectomesenchymal tissues in these tumours using antibodies to vimentin, desmin, neurofilament, and glial fibrillary acidic protein, we immunohistochemically examined nestin expression.
Results: No differentiation towards muscle and nervous tissues was found in the odontogenic ectomesenchymal tissues. Although almost all the ameloblastomas and malignant ameloblastomas were negative for nestin, odontogenic ectomesenchyme in the odontogenic mixed tumours demonstrated nestin immunolocalisation, particularly in the region adjacent to the odontogenic epithelium. Odontoblasts and their processes, pulp cells near the positive odontoblasts, and flat cells adhering to the dentine showed immunoreaction with nestin in the odontomas and odontoma-like component in the ameloblastic fibro-odontomas. Neoplastic cells in almost half cases of jaw myxoma and one case of odontogenic fibroma expressed nestin.
Conclusions: The distribution of nestin in the odontogenic mixed tumours suggests that nestin expression in the odontogenic ectomesenchyme is upregulated by stimulation from odontogenic epithelium. In addition, nestin may also be involved in the differentiation from pulp cells to odontoblasts in odontogenic tumours. Therefore, nestin is a useful marker for the odontogenic ectomesenchyme and odontoblasts in odontogenic tumours.

Nestin, one of the intermediate filaments constituting the cytoskeleton, is a marker of neural stem cells or progenitor cells. Its expression is also related to tooth development and repair of dentine.
Aims: The aim of this study was to investigate nestin expression in various odontogenic tumours and evaluate its usefulness for histopathological diagnosis.
Methods: We studied formalin fixed, paraffin embedded specimens from 129 cases of odontogenic tumours and 9 of mandibular intraosseous myxoma. After characterisation of odontogenic ectomesenchymal tissues in these tumours using antibodies to vimentin, desmin, neurofilament, and glial fibrillary acidic protein, we immunohistochemically examined nestin expression.
Results: No differentiation towards muscle and nervous tissues was found in the odontogenic ectomesenchymal tissues. Although almost all the ameloblastomas and malignant ameloblastomas were negative for nestin, odontogenic ectomesenchyme in the odontogenic mixed tumours demonstrated nestin immunolocalisation, particularly in the region adjacent to the odontogenic epithelium. Odontoblasts and their processes, pulp cells near the positive odontoblasts, and flat cells adhering to the dentine showed immunoreaction with nestin in the odontomas and odontoma-like component in the ameloblastic fibro-odontomas. Neoplastic cells in almost half cases of jaw myxoma and one case of odontogenic fibroma expressed nestin.
Conclusions: The distribution of nestin in the odontogenic mixed tumours suggests that nestin expression in the odontogenic ectomesenchyme is upregulated by stimulation from odontogenic epithelium. In addition, nestin may also be involved in the differentiation from pulp cells to odontoblasts in odontogenic tumours. Therefore, nestin is a useful marker for the odontogenic ectomesenchyme and odontoblasts in odontogenic tumours.

See end of article for authors' affiliations

Correspondence to: Dr S Fujita, Division of Oral Pathology and Bone Metabolism, Department of Developmental and Reconstructive Medicine, Nagasaki University Graduate School of Biomedical Sciences, 1-7-1 Sakamoto, Nagasaki 852-8588, Japan; fujishu@net.nagasaki-u.ac.jp

Accepted for publication 14 June 2005

Nestin is one of the intermediate filaments constituting the cytoskeleton and is known as a marker of neural stem cells or progenitor cells.[1] This protein appears at an early developmental stage of both the central nervous system and muscles. Although the function of nestin in cell differentiation is not clearly understood, nestin is replaced with glial fibrillary acidic protein (GFAP) and desmin, accompanied by developmental processing of nervous and muscular tissues, respectively.[1–3] Nestin expression has been reported in other tissues and pathological conditions, such as neural crest,[1] heart,[4] testis,[5] reactive astrocytes after brain injury,[6–9] and central and peripheral nervous system tumours.[10–12]

With respect to tooth development and dental pathological conditions, odontoblasts producing dentine in the human and rodent tooth germ express nestin.[13 14] Dentinal fibres and pulp cells adjacent to the odontoblasts at the tooth cusp

Abbreviations: AOT, adenomatoid odontogenic tumour; GFAP, glial fibrillary acidic protein

Table 1 Categories of tumour

Benign
Tumours comprising odontogenic epithelium without odontogenic ectomesenchyme (for example, ameloblastoma)
Tumours comprising odontogenic epithelium with odontogenic ectomesenchyme, with or without dental hard tissue formation (for example, ameloblastic fibroma, ameloblastic fibro-odontoma, ameloblastic fibrodentinoma, odontoma and adenomatoid odontogenic tumour)
Tumours comprising odontogenic ectomesenchyme with or without odontogenic epithelium (for example, odontogenic fibroma and myxoma)
Malignant
Odontogenic carcinomas (for example, malignant ameloblastoma)
Odontogenic sarcomas (for example, ameloblastic fibrosarcoma)
Odontogenic carcinosarcoma

regions also indicate localisation of nestin. Human nestin expression continues during tooth development and disappears when development is complete.[13] In the mature tooth with caries or after cavity formation, nestin is re-upregulated in odontoblasts and their processes when they are stimulated by caries or when they form the secondary dentine after injury, respectively.[13 15 16] Thus, nestin is considered to be related to the differentiation toward odontoblasts and to the acquisition of the function to produce dentine.

In this study, we immunohistochemically investigated nestin expression in varied odontogenic tumours. Odontogenic neoplasms are histologically divided into several categories depending on their constituting components by WHO as detailed in table 1.[17] The neoplasms indicated within parentheses were the objective materials of our study, although there is no conclusive evidence that the jaw myxomas examined in our study are derived from odontogenic organs. We found a characteristic nestin distribution in all these tumours and discussed the implication of its expression in the odontogenic tumours.

MATERIALS AND METHODS

We investigated 129 cases of human odontogenic tumours: ameloblastoma (44), malignant ameloblastoma (3), odontoma (compound type 40; complex type 22), ameloblastic fibroma (2), ameloblastic fibro-odontoma and fibrodentinoma (7), ameloblastic fibrosarcoma (2), adenomatoid odontogenic tumour (AOT) (6), and odontogenic fibroma (3). In addition, nine cases of intraosseous myxoma in the mandible were also examined. These materials were retrieved from the histopathological files of Division of Oral Pathology and Bone Metabolism, Department of Developmental and Reconstructive Medicine, Nagasaki University Graduate School of Biomedical Sciences. The specimens were fixed in 10% neutral buffered formalin fixative, decalcified with formic acid where necessary, embedded in paraffin, cut into 3 μm thick sections, and stained with haematoxylin and eosin. Table 2 summarises the clinical data of all the patients.

Table 2 Examined odontogenic tumours and jaw myxoma

Histology	No. of cases	Sex		Average age at first visit
		Male	Female	
Ameloblastoma	44	26	18	35.4
Malignant ameloblastoma	3	2	1	53.0
Odontoma	62	29	33	23.2
Compound type	40	17	23	21.1
Complex type	22	12	10	26.7
Ameloblastic fibroma	2	1	1	21.0
AFO and AFD	7	5	2	13.3
Ameloblastic fibrosarcoma	2	1	1	26.5
AOT	6	2	4	19.8
Odontogenic fibroma	3	1	2	36.7
Myxoma	9	5	4	41.7
Total	138	72	66	

AFO and AFD, ameloblastic fibro-odontoma and fibrodentinoma; AOT, adenomatoid odontogenic tumour.

To confirm that the odontogenic ectomesenchymal tissues in these tumours contain no nervous and muscular tissues, immunostaining for vimentin, desmin, neurofilament, and GFAP were performed, because muscular and neural cells frequently react with antibodies to nestin. All monoclonal antibodies against these proteins were purchased from DakoCytomation Co. Ltd, Kyoto, Japan. The immunohistochemical assay was performed using the EnVision+ system (DakoCytomation) with goat anti-mouse immunoglobulin conjugated to peroxidase labelled dextran polymer.

For the investigation of nestin expression, we used rabbit anti-human nestin polyclonal antibody (Chemicon International Inc., CA, USA) as a primary antibody, and the EnVision+ system (DakoCytomation) for polyclonal antibody. The chromogen 3,3'-diaminobenzidine (Sigma-Aldrich Japan, Tokyo, Japan) was used to reveal the sites of peroxidase activity. After the sections were counterstained with haematoxylin, they were dehydrated and mounted in a synthetic medium.

RESULTS

Characterisation of odontogenic ectomesenchymal tissues

Odontogenic ectomesenchyme and pulp tissue included in the odontogenic mixed tumours, and the odontomas were positive for vimentin and negative for desmin, neurofilament, and GFAP (supplemental fig 1; http://www.jclinpath.com/supplemental). We found that intrinsic muscle and nervous tissues showed desmin expression, and neurofilament and GFAP expression, respectively (supplemental fig 2; http://www.jclinpath.com/supplemental).

Immunohistochemical assay for nestin

A brief summary of the results is shown in table 3.

Ameloblastoma

The parenchyma of almost all the cases (43 of 44) of ameloblastoma displayed no nestin immunoexpression (fig 1). However, one case showed the expression in the cytoplasm of the focal peripheral columnar epithelium bordering the fibrous stroma.

Malignant ameloblastoma

No localisation of nestin was observed in the parenchyma of all three cases of malignant ameloblastoma.

Odontoma

Nestin immunoreactivity was found in the columnar odontoblasts adjacent to the dentine matrix, particularly in the compound-type odontomas. The positive odontoblasts were arranged in a palisading pattern on the predentine or dentine. Dentinal fibres through the dental tubules extending from the odontoblasts also showed immunoreactivity, and pulp cells adjacent to the odontoblasts were positive for nestin in some cases (fig 2). In addition, in complex-type odontomas, sparse flat cells adhering to the dentine and their processes in the irregular dental tubules were positive. Of 40 compound odontomas, 33 cases were positive, as were 16 of 22 complex odontomas.

Table 3 Expression of nestin in odontogenic tumours and jaw myxoma

Histology (no. of cases)	No. of positive cases	Localisation in parenchyma
Ameloblastoma (44)	1 (2%)	Peripheral columnar cells
Malignant ameloblastoma (3)	0 (0)	No localisation
Odontoma (62)	49 (79)	
Compound type (40)	33 (82)	Odontoblasts, dentinal fibres, pulp cells associated with odontoblasts
Complex type (22)	16 (73)	Cells adhering to dentine, their processes in dentinal tubules
Ameloblastic fibroma (2)	2 (100)	Ectomesenchyme > epithelium
AFO (7) and AFD	6 (86)	Ectomesenchyme > epithelium
Ameloblastic fibrosarcoma (2)	2 (100)	Ectomesenchyme
AOT (6)	5 (83)	Small nodular foci and rosette patterns
Odontogenic fibroma (3)	1 (33)	Ectomesenchyme
Myxoma (9)	4 (44)	Tumour cells homogenously in positive cases

AFO and AFD, ameloblastic fibro-odontoma and fibrodentinoma; AOT, adenomatoid odontogenic tumour.

Ameloblastic fibroma

Odontogenic ectomesenchymal tissues in the ameloblastic fibromas demonstrated immunoreactivity for nestin, although they did not contain the differentiated odontoblasts. Foci of aggregation of positive cells were noted in the ectomesenchymal element. As an intriguing finding, the ectomesenchymal cells around the neoplastic follicular odontogenic epithelium showed intense reaction with nestin, and the intensity weakened with greater distance from the odontogenic epithelium (fig 3). Some follicular epithelial components showed a cytoplasmic reaction in the peripheral columnar and inner stellate cells.

Ameloblastic fibro-odontoma and fibrodentinoma

The localisation of nestin in the ameloblastic fibro-odontomas and ameloblastic fibrodentinomas mimicked that in the ameloblastic fibromas and odontomas. The focal areas in the odontogenic ectomesenchymal tissue, particularly near the epithelial elements, showed strong reactivity. Some of the follicular patterns of epithelial elements demonstrated nestin immunoreactivity. Odontoma components showed nestin expression in differentiated odontoblasts, their processes, and adjacent pulp cells. Nestin localisation was also seen in the flat to plump cells adhering the dentinoid matrix and in sparse dentinal fibres in ameloblastic fibrodentinomas (fig 4).

Ameloblastic fibrosarcoma

Odontogenic ectomesenchymal cells were positive for nestin, although epithelial components were negative in all cases.

AOT

Five of six cases of AOT indicated intense nestin expression in epithelial elements, unlike the odontogenic mixed tumours, which showed immunoreactivity principally in the ectomesenchymal tissue. Nestin was intensely expressed in small nodular areas and in rosette arrangements in the epithelial elements of AOT (fig 5A). These positive cells localised near the droplet extracellular depositions, and haematoxylin and eosin revealed amorphous eosinophilic characteristics (fig 5B, C).

Odontogenic fibroma

Of the three cases of odontogenic fibroma, one had odontogenic ectomesenchymal cells that were positive for nestin. This specimen contained abundant odontogenic epithelial strands, and the positive cells presented near the odontogenic epithelium.

Myxoma

Four of the nine cases of myxoma displayed round, angular, or reticular neoplastic cells in the myxoid stroma that were positive for nestin (fig 6). One positive case included

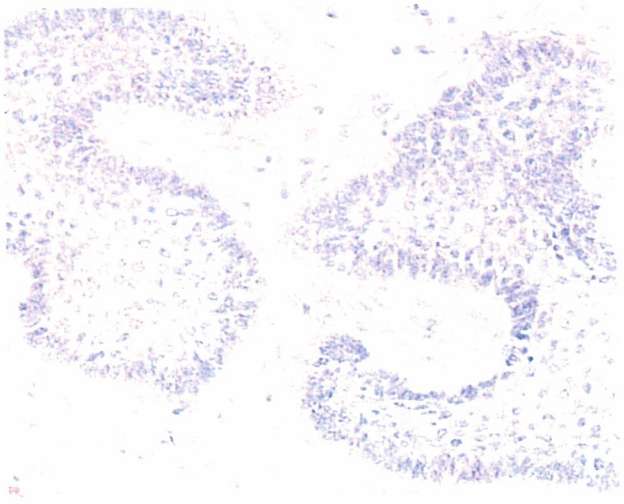

Figure 1 Parenchyma and stoma cells of ameloblastoma showed no nestin immunoreactivity.

Figure 2 Odontoma showed nestin expression in the odontoblasts and their processes in the dental tubules. Pulp cells adjacent to the odontoblasts gave a positive reaction (arrows).